A.T.E.I. of Thessaloniki

School of Technological Applications

Department of Information Technology

Biomedical signal analysis using blind signal processing methods

Final Thesis

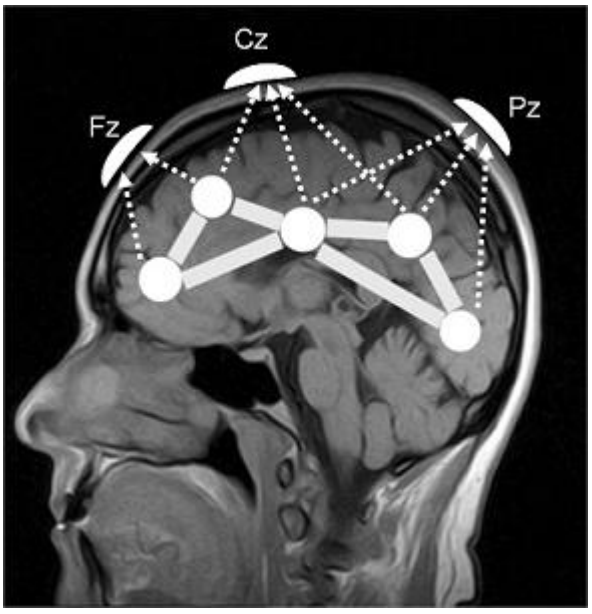

Student: Gabriela Vranou

Supervisor: Konstantinos I. Diamantaras

Thessaloniki 2013

1 Table of Contents

Table of Figures

Preface

This thesis has the goal of presenting most of the different kinds of Biomedical Signals as of this date, various methods of Blind Signal Processing and examples of their application.

The work put on writing it consisted of two parts:

- Bibliographic study of the mentioned methods, understanding the various problems that these methods are used on and finding respective tools.
- Finding databases of biomedical signals and application of selected methods in selected signals.

It is organized in five sections:

1. Biomedical Signals
2. Blind Signal Processing
3. Application
4. Bibliography and Recommended reading
5. Appendix

2 Biomedical Signals

Living organisms are made up of many component systems — the human body, for example, includes the nervous system, the cardiovascular system, and the musculoskeletal system, among others. Each system is made up of several subsystems that carry on many physiological processes.

Physiological processes are complex phenomena, including nervous or hormonal stimulation and control; inputs and outputs that could be in the form of physical material, neurotransmitters, or information; and action that could be mechanical, electrical, or biochemical. Most physiological processes are accompanied by or manifest themselves as signals that reflect their nature and activities. Such signals could be of many types, including biochemical in the form of hormones and neurotransmitters, electrical in the form of potential or current, and physical in the form of pressure or temperature.

Diseases or defects in a biological system cause alterations in its normal physiological processes, leading to pathological processes that affect the performance, health, and general well-being of the system. A pathological process is typically associated with signals that are different in some respects from the corresponding normal signals. If we possess a good understanding of a system of interest, it becomes possible to observe the corresponding signals and assess the state of the system. The task is not very difficult when the signal is simple and appears at the outer surface of the body, but as the source deepens or the signal itself is really faint, more complex methods/tools are needed.

Some of the most important biomedical signals are recorded using Electrocardiogram (ECG), Electroencephalogram (EEG), Magnetoencephalogram (MEG) and also imaging methods as Magnetic Resonance Imaging (MRI) and Positron emission tomography (PET). Most of these methods will be presented and compared through this chapter.

2.1 Electrocardiogram (ECG)

Electrocardiography is a transthoracic interpretation of the electrical activity of the heart over a period of time, as detected by electrodes attached to the outer surface of the skin and recorded by a device external to the body. The recording produced by this noninvasive procedure is termed as electrocardiogram (ECG or EKG).

An ECG test records the electrical activity of the heart; it is used to measure the rate and regularity of heartbeats, as well as the size and position of the chambers, the presence of any damage to the heart, and the effects of drugs or devices used to regulate the heart, such as a pacemaker.

Specifically, the ECG device detects and amplifies the tiny electrical changes on the skin that are caused when the heart muscle depolarizes during each heartbeat. At rest, each heart muscle cell has a negative charge, called the membrane potential, across its cell membrane. Decreasing this negative charge towards zero, via the influx of the positive cations, Na+ and Ca++, is called depolarization, which activates the mechanisms in the cell that cause it to contract. During each heartbeat, a healthy heart will have an orderly progression of a wave of depolarisation that is triggered by the cells in the sinoatrial node, spreads out through the atrium, passes through the atrioventracular node and then spreads all over the ventricles. This is detected as tiny rises and falls in the voltage between two electrodes placed either side of the heart which is displayed as a wavy line either on a screen or on paper. This display indicates the overall rhythm of the heart and weaknesses in different parts of the heart muscle. (Braunwald, 1997)

Usually, more than two electrodes are used, and they can be combined into a number of pairs. The output from each pair is known as a lead. Each lead looks at the heart from a different angle, as shown on Figure 2-1. Different types of ECGs can be referred to by the number of leads that are recorded, for example 3-lead, 5-lead or 12-lead ECGs (sometimes simply "a 12-lead").

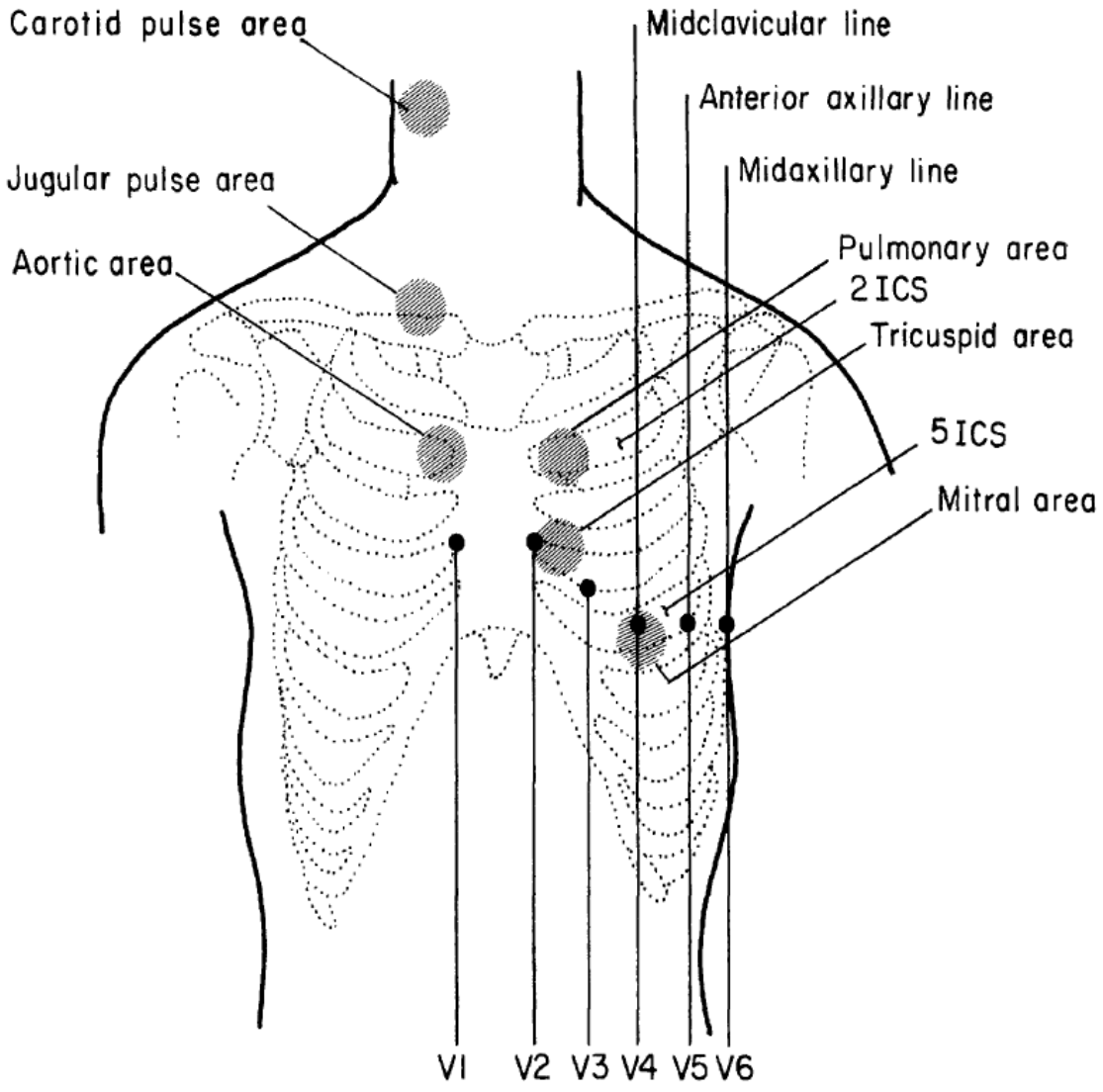

Figure 2-1 Positions for placement of the precordial (chest) leads VI - V6 for ECG, auscultation areas for heart sounds, and pulse transducer positions for the carotid and jugular pulse signals. ICS: intercostal space.

A typical ECG tracing of the cardiac cycle (heartbeat) consists of a P wave, a QRS complex, a T wave, and a U wave as shown on Figure 2-2 and described on Table 2-1. The baseline voltage of the electrocardiogram is known as the isoelectric line. Typically, the isoelectric line is measured as the portion of the tracing following the T wave and preceding the next P wave. The baseline of the electrocardiogram (the flat horizontal segments) is measured as the portion of the tracing following the T wave

and preceding the next P wave and the segment between the P wave and the following QRS complex (PR segment). (Hurst, 1998)

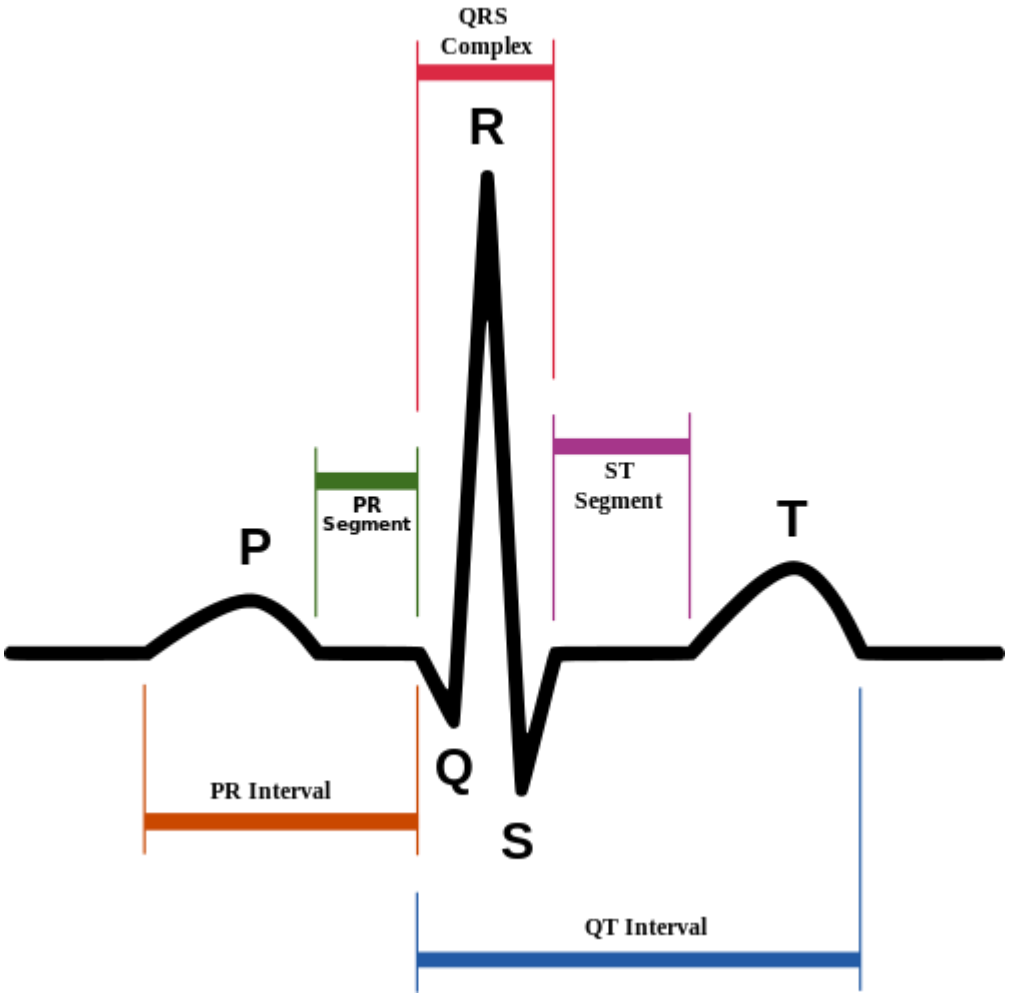

Figure 2-2 Schematic representation of normal ECG

In a normal healthy heart, the baseline is equivalent to the isoelectric line (0mV) and represents the periods in the cardiac cycle when there are no currents flowing towards either the positive or negative ends of the ECG leads. However, in a diseased heart the baseline may be elevated (e.g. cardiac ischaemia) or depressed (e.g. myocardial infarction) relative to the isoelectric line due to injury currents flowing during the TP and PR intervals when the ventricles are at rest. The ST segment typically remains close to the isoelectric line as this is the period when the ventricles are fully depolarised and thus no currents can flow in the ECG leads.

Table 2-1 Description of intervals and waves of an ECG signal

Feature	Description	Duration
RR interval	The interval between an R wave and the next R wave: Normal resting heart rate is between 60 and 100 bpm.	0.6 to 1.2s
P wave	During normal atrial depolarization, the main electrical vector is directed from the SA node towards the AV node, and spreads from the right atrium to the left atrium. This turns into the P wave on the ECG.	80ms
PR interval	The PR interval is measured from the beginning of the P wave to the beginning of the QRS complex. The PR interval reflects the time the electrical impulse takes to travel from the sinus node through the AV node and entering the ventricles. The PR interval is, therefore, a good estimate of AV node function.	120 to 200ms
PR segment	The PR segment connects the P wave and the QRS complex. The impulse vector is from the AV node to the bundle of His to the bundle branches and then to the Purkinje fibers. This electrical activity does not produce a contraction directly and is merely traveling down towards the ventricles, and this shows up flat on the ECG. The PR interval is more clinically relevant.	50 to 120ms
QRS complex	The QRS complex reflects the rapid depolarization of the right and left ventricles. They have a large muscle mass compared to the atria, so the QRS complex usually has a much larger amplitude than the P-wave.	80 to 120ms
J-point	The point at which the QRS complex finishes and the ST segment begins, it is used to measure the degree of ST elevation or depression present.	N/A

Feature	Description	Duration
ST segment	The ST segment connects the QRS complex and the T wave. The ST segment represents the period when the ventricles are depolarized. It is isoelectric.	80 to 120ms
T wave	The T wave represents the repolarization (or recovery) of the ventricles. The interval from the beginning of the QRS complex to the apex of the T wave is referred to as the absolute refractory period. The last half of the T wave is referred to as the relative refractory period (or vulnerable period).	160ms
ST interval	The ST interval is measured from the J point to the end of the T wave.	320ms
QT interval	The QT interval is measured from the beginning of the QRS complex to the end of the T wave. A prolonged QT interval is a risk factor for ventricular tachyarrhythmias and sudden death. It varies with heart rate and for clinical relevance requires a correction for this, giving the QTc.	Up to 420ms in heart rate of 60 bpm
U wave	The U wave is hypothesized to be caused by the repolarization of the interventricular septum. They normally have a low amplitude, and even more often completely absent. They always follow the T wave and also follow the same direction in amplitude. If they are too prominent, suspect hypokalemia, hypercalcaemia or hyperthyroidism usually.	
J wave	The J wave, elevated J-point or Osborn wave appears as a late delta wave following the QRS or as a small secondary R wave. It is considered pathognomonic of hypothermia or hypocalcaemia.	

2.2 Electroencephalogram (EEG)

The electroencephalogram (EEG) is a record of the oscillations of brain electric potentials recorded from electrodes attached to the human scalp (Niedermeyer and da Silva, 2004). The EEG reveals synaptic action that is moderately to strongly correlated with brain state. Most EEG signals originate in the brain's outer layer (the cerebral cortex), believed largely responsible for our individual thoughts, emotions and behavior. Cortical synaptic action generates electrical signals that change in the 10 to 100 millisecond range.

EEG and MEG (Magnetoencephalography) are the only widely available technologies with sufficient temporal resolution to follow these fast dynamic changes. On the other hand, EEG and MEG spatial resolutions are poor relative to modern brain structural imaging methods like computer tomography (CT), positron emitted tomography (PET) and magnetic resonance imaging (MRI) as the electric potential generated by a single neuron is far too small to be picked up by EEG or MEG (Nunez, 1981).

Electrodes are placed inside the skull to study non-human mammals or human epilepsy patients. Such intracranial recordings provide measures of cortical dynamics at several small scales depending on electrode size. By contrast, scalp recorded EEG dynamics is exclusively large scale and nearly independent of electrode size because of the severe space averaging between brain current sources and scalp electrodes. The technical and ethical limitations of human intracranial recording force emphasis on scalp recordings. Luckily, these large-scale estimates provide important measures of brain dysfunction for clinical work and cognition or behavior for basic scientific studies.

Each scalp electrode (or MEG coil) records electrical activity at very large scales, recording electric potentials (or magnetic fields) generated in tissue containing something like 10 million to one billion neurons in the cortical layer. Therefore, EEG activity always reflects the summation of the synchronous activity of thousands or

millions of neurons that have similar spatial orientation. If the cells do not have similar spatial orientation, their ions do not line up and create waves to be detected. Pyramidal neurons of the cortex are thought to produce the most EEG signal because they are well-aligned and fire together. Because voltage fields fall off with the square of distance, activity from deep sources is more difficult to detect than currents near the skull (Klein, Thorne, 2006).

2.2.1 Recording Methods

In conventional scalp EEG, the recording is obtained by placing electrodes, with diameters typically in the 0.4 to 1.0 cm range, on the scalp with a conductive gel or paste, usually after preparing the scalp area by light abrasion to reduce impedance due to dead skin cells. Many systems typically use electrodes, each of which is attached to an individual wire. Some systems use caps or nets into which electrodes are embedded; this is particularly common when high-density arrays of electrodes are needed. In standard clinical practice, 19 recording electrodes are placed uniformly over the scalp (the International 10-20 System). In addition, one or two reference electrodes (often placed on ear lobes) and a ground electrode (often placed on the nose to provide amplifiers with reference voltages) are required.

Each electrode is connected to one input of a differential amplifier (one amplifier per pair of electrodes); a common system reference electrode is connected to the other input of each differential amplifier. These amplifiers amplify the voltage between the active electrode and the reference (typically 1,000–100,000 times, or 60–100 dB of voltage gain). The digital EEG signal is stored electronically and can be filtered for display. Typical settings for the high-pass filter and a low-pass filter are 0.5-1 Hz and 35–70 Hz, respectively. The high-pass filter typically filters out slow artifact, such as electrogalvanic signals and movement artifact, whereas the low-pass filter filters out high-frequency artifacts, such as electromyographic signals. An additional notch filter is typically used to remove artifact caused by electrical power.

During the recording, a series of activation procedures may be used. These procedures may induce normal or abnormal EEG activity that might not otherwise be

seen. These procedures include hyperventilation, photic stimulation (with a strobe light), eye closure, mental activity, sleep and sleep deprivation. During (inpatient) epilepsy monitoring, a patient's typical seizure medications may be withdrawn.

The resulting multi-channel data are submitted to algorithms that estimate potentials on the brain surface by accounting for distortions caused by intervening tissue and the physical separation of electrodes from brain. The combined use of high electrode density and computer algorithms providing such "inward continuation estimates" to the brain surface is called high resolution EEG. Another approach using computer methods is dipole localization. This method can estimate the location of source regions in the brain depths in a few specialized applications where EEG is mainly generated in only one or two isolated source regions.

In referential recordings, potentials between each recording electrode and a fixed reference are measured over time. The distinction between "recording" and "reference" electrodes is mostly artificial since both electrode categories involve potential differences between body sites, allowing closed current loops through tissue and EEG machine. Bipolar recordings measure potential differences between adjacent scalp electrodes. When such bipolar electrodes are placed close together (say 1 or 2 centimeters), potential differences are estimates of tangential electric fields (or current densities) in the scalp between the electrodes. Electrode placements and the different ways of combining electrode pairs to measure potential differences on the head constitute the electrode montage.

Any single electrode may be chosen as the reference and potentials at other locations recorded with respect to this reference. In EEG practice, inappropriate reference choices have often led to erroneous interpretations of brain source locations and measures of dynamic behavior. When large numbers of electrodes are employed, potential at each location may be measured with respect to the average of all potentials (the common average reference), which often provides a good estimate of potential at infinity. The common average reference is not appropriate when electrode coverage is sparse (perhaps less than 64 electrodes).

Derivatives of the EEG technique include evoked potentials (EP), which involves averaging the EEG activity time-locked to the presentation of a stimulus of some sort (visual, somatosensory, or auditory). Event-related potentials (ERPs) refer to averaged EEG responses that are time-locked to more complex processing of stimuli; this technique is used in cognitive science, cognitive psychology, and psychophysiological research.

2.2.2 International 10–20 system

Electrode locations and names are specified by the International 10–20 system (Figure 1-2) for most clinical and research applications. This system ensures that the naming of electrodes is consistent across laboratories.

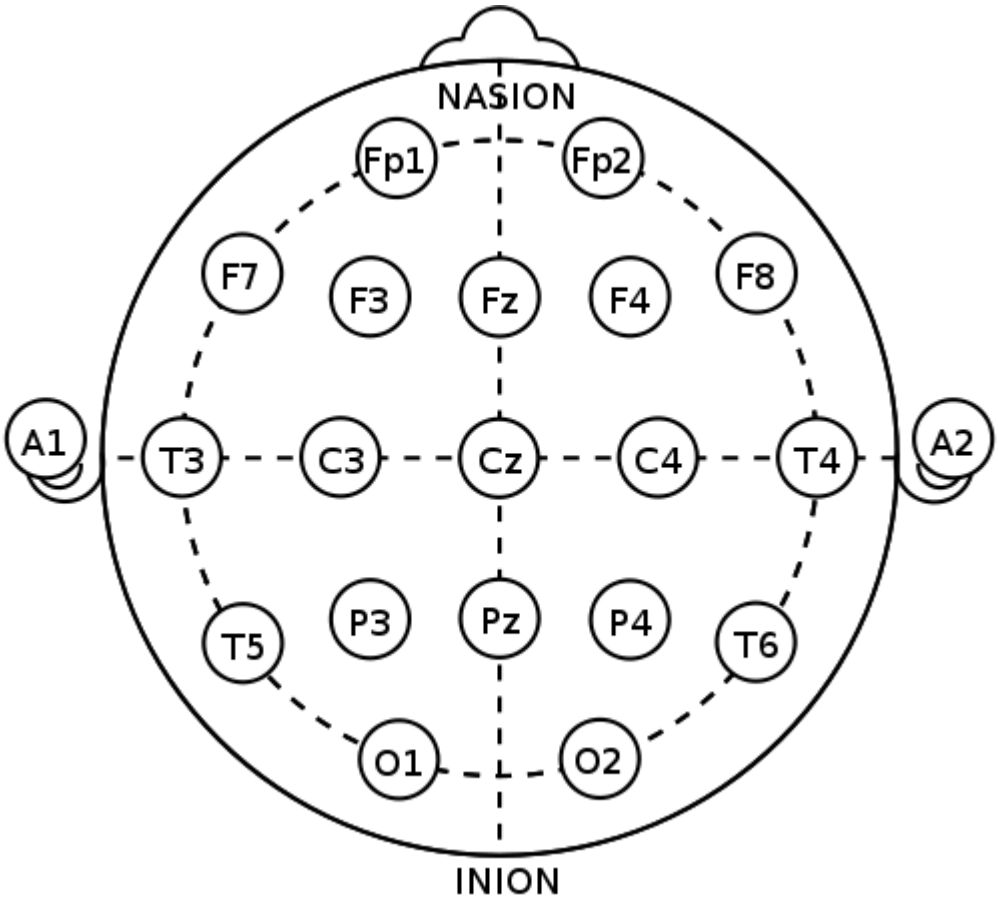

Figure 2-3 The 10-20 system or International 10-20 system

This system is based on the relationship between the location of an electrode and the underlying area of cerebral cortex. The "10" and "20" refer to the fact that the actual distances between adjacent electrodes are either 10% or 20% of the total front-back or right-left distance of the skull.

Each site has a letter to identify the lobe and a number to identify the hemisphere location. The letters F, T, C, P and O stand for frontal, temporal, central, parietal, and occipital lobes, respectively. Note that there exists no central lobe; the "C" letter is only used for identification purposes only. A "z" (zero) refers to an electrode placed on the midline. Even numbers (2,4,6,8) refer to electrode positions on the right hemisphere, whereas odd numbers (1,3,5,7) refer to those on the left hemisphere.

Two anatomical landmarks are used for the essential positioning of the EEG electrodes: first, the nasion which is the distinctly depressed area between the eyes, just above the bridge of the nose; second, the inion, which is the lowest point of the skull from the back of the head and is normally indicated by a prominent bump (Towle et al., 1993).

2.2.3 Waves and Artifacts

The EEG is typically described in terms of rhythmic activity and transients. The rhythmic activity is divided into bands by frequency. Scalp EEG activity shows oscillations at a variety of frequencies. To some degree, these frequency bands are a matter of nomenclature (i.e., any rhythmic activity between 6–12 Hz can be described as "alpha"), but these designations arose because rhythmic activity within a certain frequency range was noted to have characteristic frequency ranges, spatial distributions and are associated with different states of brain functioning (e.g., waking and the various sleep stages). These oscillations represent synchronized activity over a network of neurons (see Table 2-2). The neuronal networks underlying some of these oscillations are understood (e.g., the thalamocortical resonance underlying sleep spindles), while many others are not (e.g., the system that generates the posterior basic rhythm) (Whittingstall and Logothetis, 2009)

Table 2-2 Comparison of EEG bands

Band	Frequency	Location	Normally	Pathologically
Delta	up to 4 Hz	frontally in adults, posteriorly in children; high-amplitude waves	adult slow-wave sleep in babies Has been found during some continuous-attention tasks	subcortical lesions diffuse lesions metabolic encephalopathy hydrocephalus deep midline lesions
Theta	4 – 8 Hz	Found in locations not related to task at hand	young children drowsiness or arousal in older children and adults idling Associated with inhibition of elicited responses (has been found to spike in situations where a person is actively trying to repress a response or action).	focal subcortical lesions metabolic encephalopathy deep midline disorders some instances of hydrocephalus
Alpha	8 – 13 Hz	Posterior regions of head, both sides, higher in amplitude on non-dominant side. Central sites (c3-c4) at rest	relaxed/reflecting closing the eyes Also associated with inhibition control, seemingly with the purpose of timing inhibitory activity in different locations across the brain.	coma

Band	Frequency	Location	Normally	Pathologically
Beta	>13 – 30 Hz	both sides, symmetrical distribution, most evident frontally; low-amplitude waves	alert active, busy, or anxious thinking, active concentration	benzodiazepines
Gamma	30 – 100+ Hz	Somatosensory cortex	Displays during cross-modal sensory processing (perception that combines two different senses, such as sound and sight) Also is shown during short-term memory matching of recognized objects, sounds, or tactile sensations	A decrease in gamma-band activity may be associated with cognitive decline, especially when related to the theta band; however, this has not been proven for use as a clinical diagnostic measurement
Mu	8 – 13 Hz	Sensorimotor cortex	Shows rest-state motor neurons.	Mu suppression could indicate that motor mirror neurons are working. Deficits in Mu suppression, and thus in mirror neurons, might play a role in autism.

Some features of the EEG are transient rather than rhythmic. Spikes and sharp waves may represent seizure activity or interictal activity in individuals with epilepsy or a predisposition toward epilepsy. Other transient features are normal: vertex waves and sleep spindles are seen in normal sleep. Note that there are types of activity that

are statistically uncommon, but not associated with dysfunction or disease. These are often referred to as "normal variants." The mu rhythm is an example of a normal variant.

The normal EEG varies by age. The neonatal EEG is quite different from the adult EEG. The EEG in childhood generally has slower frequency oscillations than the adult EEG. The normal EEG also varies depending on state. The EEG is used along with other measurements (EOG, EMG) to define sleep stages in polysomnography. Stage I sleep (equivalent to drowsiness in some systems) appears on the EEG as drop-out of the posterior basic rhythm. Stage II sleep is characterized by sleep spindles—transient runs of rhythmic activity in the 12–14 Hz range (sometimes referred to as the "sigma" band) that have a frontal-central maximum. Most of the activity in Stage II is in the 3–6 Hz range. Stage III and IV sleep are defined by the presence of delta frequencies and are often referred to collectively as "slow-wave sleep." Stages I-IV comprise non-REM (or "NREM") sleep. The EEG in REM (rapid eye movement) sleep appears somewhat similar to the awake EEG.

EEG under general anesthesia depends on the type of anesthetic employed. With halogenated anesthetics, a rapid (alpha or low beta), nonreactive EEG pattern is seen over most of the scalp, especially anteriorly; in some older terminology this was known as a WAR (widespread anterior rapid) pattern, contrasted with a WAIS (widespread slow) pattern associated with high doses of opiates. Anesthetic effects on EEG signals are beginning to be understood at the level of drug actions on different kinds of synapses and the circuits that allow synchronized neuronal activity.

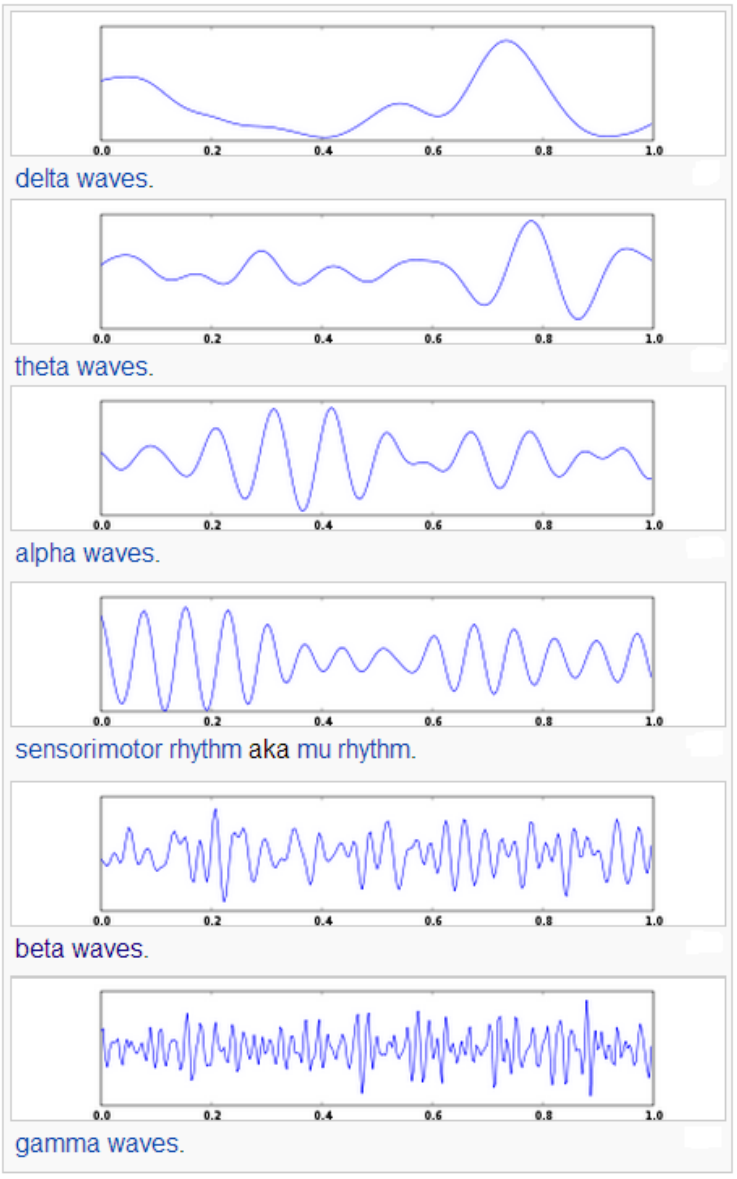

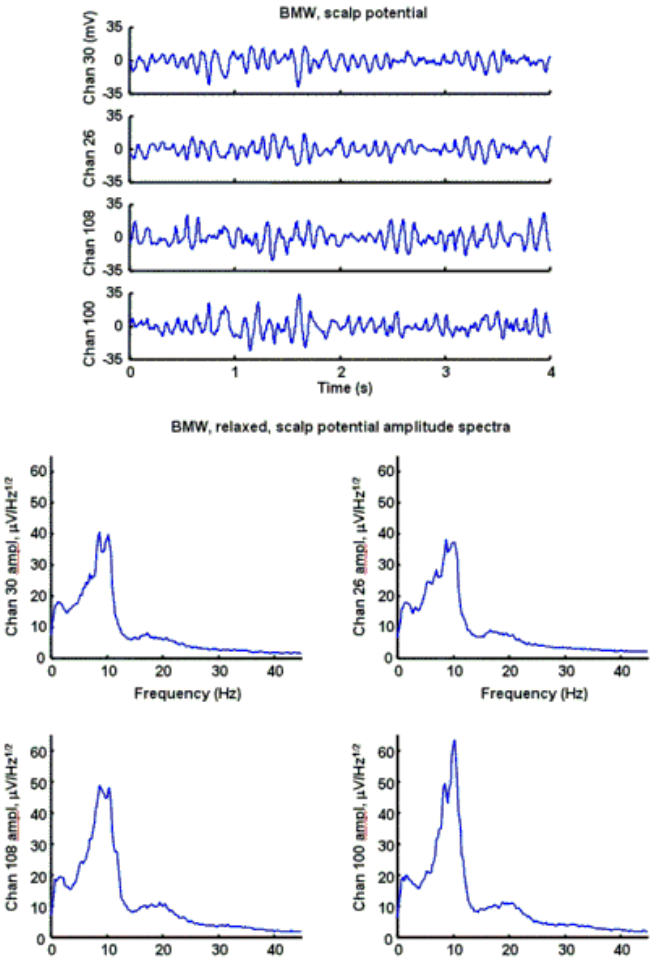

Figure 2-4 (Left) Universally recognized frequency ranges as described on Table 1-1.

(Upper Right) Alpha rhythm recorded from a healthy relaxed subject (age 25) with closed eyes using an electrode on the neck as reference. Four seconds of data are shown from four scalp locations (left frontal-channel 30; right frontal-channel 26; left posterior-channel 108; right posterior-channel 100). The amplitude is given in microvolts. This EEG was recorded at the Brain Sciences Institute in Melbourne. (Lower Right) The corresponding amplitude spectra based on the full five minute record reveals dominant activity in the alpha (8-13 Hz) band. Reproduced from Nunez and Srinivasan (2006).

Electrical signals detected along the scalp by an EEG, but that originate from non-cerebral origin are called artifacts. EEG data is almost always contaminated by such artifacts. The amplitude of artifacts can be quite large relative to the size of amplitude of the cortical signals of interest. This is one of the reasons why it takes considerable experience to correctly interpret EEGs clinically. Some of the most common types of biological artifacts include:

- Eye-induced artifacts (includes eye blinks, eye movements and extra-ocular muscle activity)
- ECG (cardiac) artifacts
- EMG (muscle activation)-induced artifacts
- Glossokinetic artifacts

Some of these artifacts can be useful in various applications. The EOG signals, for instance, can be used to detect and track eye-movements, which are very important in polysomnography, and is also in conventional EEG for assessing possible changes in alertness, drowsiness or sleep.

ECG artifacts are quite common and can be mistaken for spike activity. Because of this, modern EEG acquisition commonly includes a one-channel ECG from the extremities. This also allows the EEG to identify cardiac arrhythmias that are an important differential diagnosis to syncope or other episodic/attack disorders.

Glossokinetic artifacts are caused by the potential difference between the base and the tip of the tongue. Minor tongue movements can contaminate the EEG, especially in parkinsonian and tremor disorders.

In addition to artifacts generated by the body, many artifacts originate from outside the body. Movement by the patient, or even just settling of the electrodes, may cause electrode pops, spikes originating from a momentary change in the impedance of a

given electrode. Poor grounding of the EEG electrodes can cause significant 50 or 60 Hz artifact, depending on the local power system's frequency.

2.3 Magnetic Resonance Imaging

Magnetic Resonance Imaging, or MRI, is a method of imaging the interior of structures noninvasively. The full name, Nuclear Magnetic Resonance Imaging, usually shortened to MRI, describes the technique. If an atomic **N**ucleus is exposed to a static **M**agnetic field, it **R**esonates when a varying electromagnetic field is applied at the proper frequency. An Image is computed from the resonance signals of which the frequency and phase (timing) contain space information. MRI is important because it is noninvasive, safe, provides good contrast between the different soft tissues of the body (which makes it especially useful in imaging the brain, muscles, the heart, and cancers compared with other medical imaging techniques) and yields information that cannot be obtained with any other techniques.

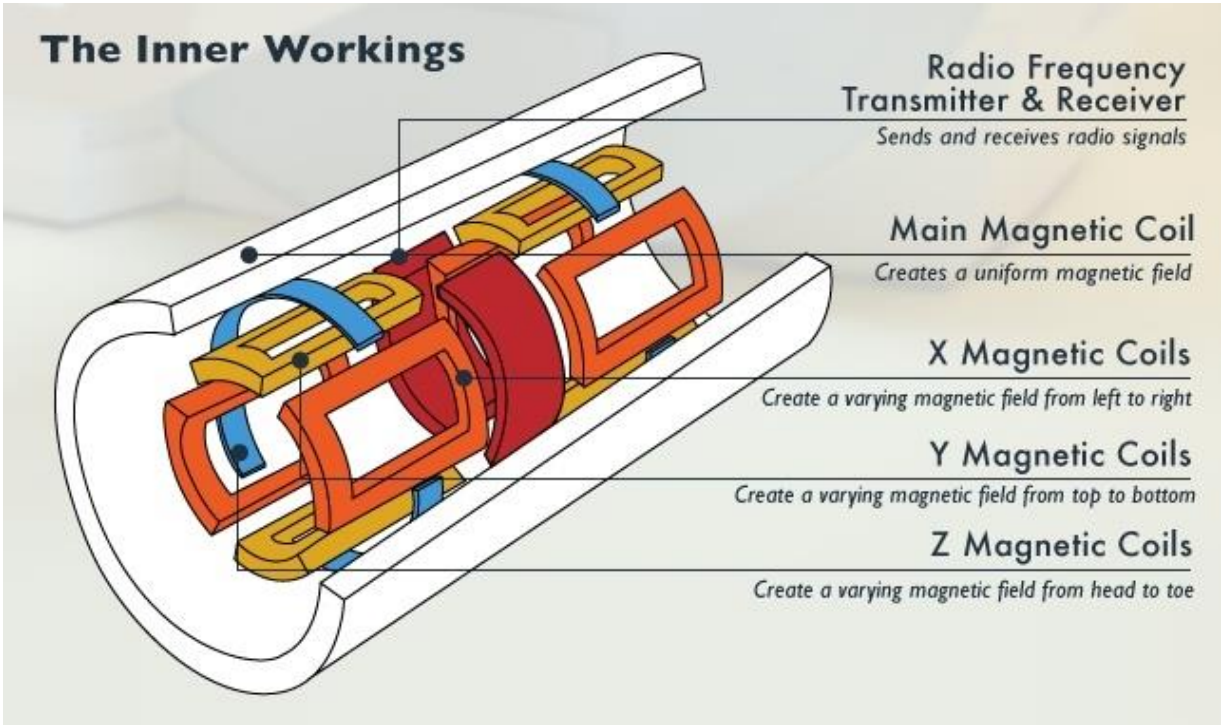

Figure 2-5 MRI Equipment

Specifically, an MRI device consists of a magnet, magnetic gradient coils, an RF (radio frequency) transmitter and receiver (see Figure 2-5), and a computer that controls the acquisition of signals and computes the MR images. The subject lies within the large, powerful magnet where the magnetic field is used to align the magnetization of some atomic nuclei in the body, and radio frequency magnetic fields are applied to systematically alter the alignment of this magnetization. This causes the nuclei to produce a rotating magnetic field detectable by the scanner—and this information is recorded to construct an image of the scanned area of the body. Magnetic field gradients cause nuclei at different locations to precess at different speeds, which allows spatial information to be recovered using Fourier analysis of the measured signal. By using gradients in different directions, 2D images or 3D volumes can be obtained in any arbitrary orientation.

One of the most important attributes of MRI, which distinguishes it from all other human imaging techniques, is the high quality of contrast, especially among soft tissues. In a typical MR image the contrast is provided by the concentration, or density, of the observed nucleus, and the exponential relaxation times of the signals following the transient B_1 pulse. Sometimes MRI contrast agents may be injected intravenously to enhance the normal contrast among soft tissues and the appearance of blood vessels, tumors or inflammation. These agents may contain a paramagnetic substance, such as gadolinium, conjugated to other moieties to make it safer in the body. Paramagnetic agents have a strong magnetic effect on the surrounding molecules and greatly enhance the image of the regions in which it is located. There are now thousands of different MRI contrast agents available for various purposes. The invention and introduction of these agents requires attention not just to the strength of contrast, but to the possibility of directing the contrast toward specific diseases (such as contrast agents that will link to receptors on the surface of cancer cells) and very importantly, to the possibility of short term or long term adverse effects of their use.

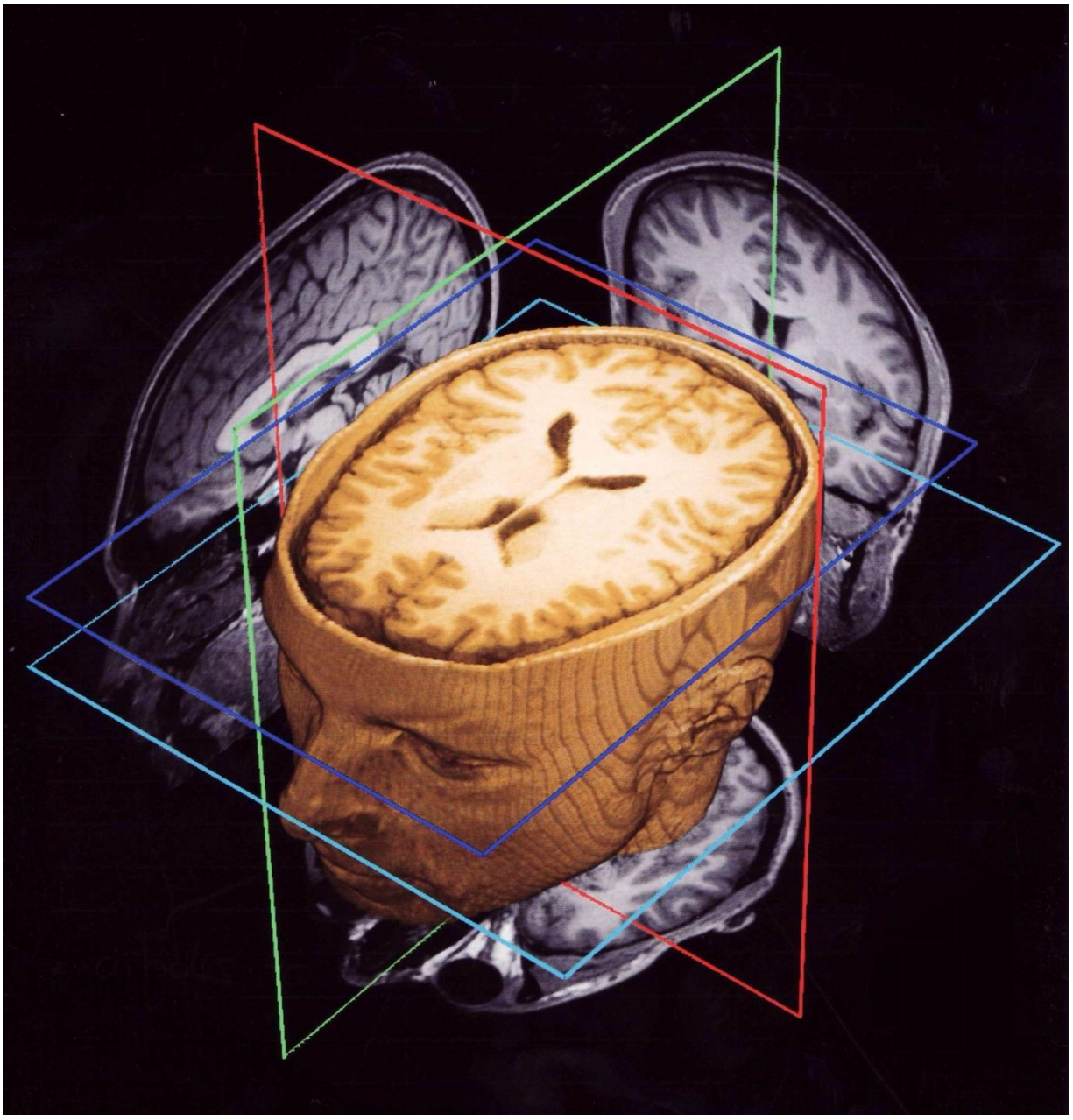

Figure 2-6 3D Head model cut on axial view and the corresponding coronal, sagittal and axial MRI scan images produced

2.3.1 Basic MRI scans

2.3.1.1 T1-weighted MRI

T_1-weighted scans refer to a set of standard scans that depict differences in the spin-lattice (or T_1) relaxation time of various tissues within the body. T_1 weighted images can be acquired using either spin echo or gradient-echo sequences. T_1-weighted contrast can be increased with the application of an inversion recovery RF pulse. Gradient-echo based T_1-weighted sequences can be acquired very rapidly because of their ability to use short inter-pulse repetition times (T_R). T_1-weighted sequences are often collected before and after infusion of T_1-shortening MRI contrast agents. In the brain T_1-weighted scans provide appreciable contrast between gray and white matter. In the body, T_1 weighted scans work well for differentiating fat from water—with water appearing darker and fat brighter.

2.3.1.2 T2-weighted MRI

T_2-weighted scans are another basic type. Like the T_1-weighted scan, fat is differentiated from water, but in this case fat shows darker, and water lighter. For example, in the case of cerebral and spinal study, the CSF (cerebrospinal fluid) will be lighter in T_2-weighted images. These scans are therefore particularly well suited to imaging edema, with long T_E and long T_R. Because the spin echo sequence is less susceptible to inhomogeneities in the magnetic field, these images have long been a clinical workhorse.

*2.3.1.3 T*2-weighted MRI*

T^*2 (pronounced "T 2 star") weighted scans use a gradient echo (GRE) sequence, with long T_E and long T_R. The gradient echo sequence used does not have the extra refocusing pulse used in spin echo so it is subject to additional losses above the normal T_2 decay (referred to as T_2'), these taken together are called T^*

2. This also makes it more prone to susceptibility losses at air/tissue boundaries, but can increase contrast for certain types of tissue, such as venous blood.

2.3.1.4 *Spin density weighted MRI*

Spin density, also called proton density, weighted scans try to have no contrast from either T_2 or T_1 decay, the only signal change coming from differences in the amount of available spins (hydrogen nuclei in water). It uses a spin echo or sometimes a gradient echo sequence, with short T_E and long T_R.

2.3.2 Specialized MRI scans

2.3.2.1 *Magnetic resonance angiography*

Magnetic resonance angiography is used to generate pictures of arteries in order to evaluate them for potential ruptures or for abnormal narrowing. MR angiography was first introduced in the late 1980s, and a number of different specific methods are now used.

Figure 2-7 Magnetic resonance angiography of human brain on axial view

2.3.2.2 *Diffusion imaging*

Diffusion MRI (or dMRI) records the rate and direction of water (or sometimes of metabolites) diffusion within body organs. The technique is useful in observation of strokes, in which the water of edema diffuses particularly freely. A variant, 'diffusion tensor imaging' or 'diffusion tractology' provides spectacular images of tracts of muscle or nerve fiber bundles, because water diffusion is much faster along the length of the fibers than across them. These images are clinically useful in showing interruption of normal fiber anatomy by tumors or trauma. More recently, a new field has emerged, diffusion functional MRI (DfMRI) as it was suggested that with dMRI one could also get images of neuronal activation in the brain.

In diffusion weighted imaging (DWI) (see Figure 1-5), the intensity of each image element (voxel) reflects the best estimate of the rate of water diffusion at that location. Because the mobility of water is driven by thermal agitation and highly dependent on its cellular environment, the hypothesis behind DWI is that findings may indicate (early) pathologic change. For instance, DWI is more sensitive to early changes after a stroke than more traditional MRI measurements such as T_1 or T_2 relaxation rates. A variant of diffusion weighted imaging, diffusion spectrum imaging (DSI), was used in deriving the Connectome data sets; DSI is a variant of diffusion-weighted imaging that is sensitive to intra-voxel heterogeneities in diffusion directions caused by crossing fiber tracts and thus allows more accurate mapping of axonal trajectories than other diffusion imaging approaches.

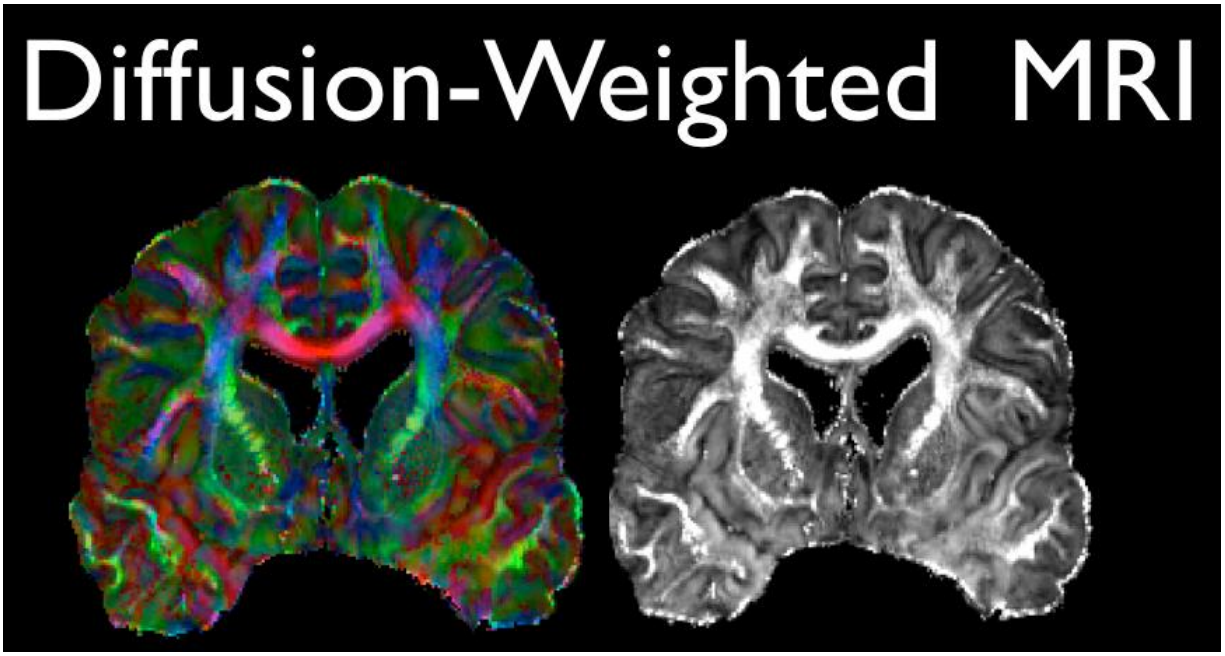

Figure 2-8 Diffusion Weighted Imaging

DWI is most applicable when the tissue of interest is dominated by isotropic water movement e.g. grey matter in the cerebral cortex and major brain nuclei, or in the body—where the diffusion rate appears to be the same when measured along any axis. However, DWI also remains sensitive to T_1 and T_2 relaxation. To entangle diffusion and relaxation effects on image contrast, one may obtain quantitative images of the diffusion coefficient, or more exactly the Apparent Diffusion Coefficient (ADC). The ADC concept was introduced to take into account the fact that the diffusion process is complex in biological tissues and reflects several different mechanisms.

Diffusion tensor imaging (DTI) (see Figure 1-6) is important when a tissue—such as the neural axons of white matter in the brain or muscle fibers in the heart—has an internal fibrous structure analogous to the anisotropy of some crystals. Water will then diffuse more rapidly in the direction aligned with the internal structure, and more slowly as it moves perpendicular to the preferred direction. This also means that the

measured rate of diffusion will differ depending on the direction from which an observer is looking.

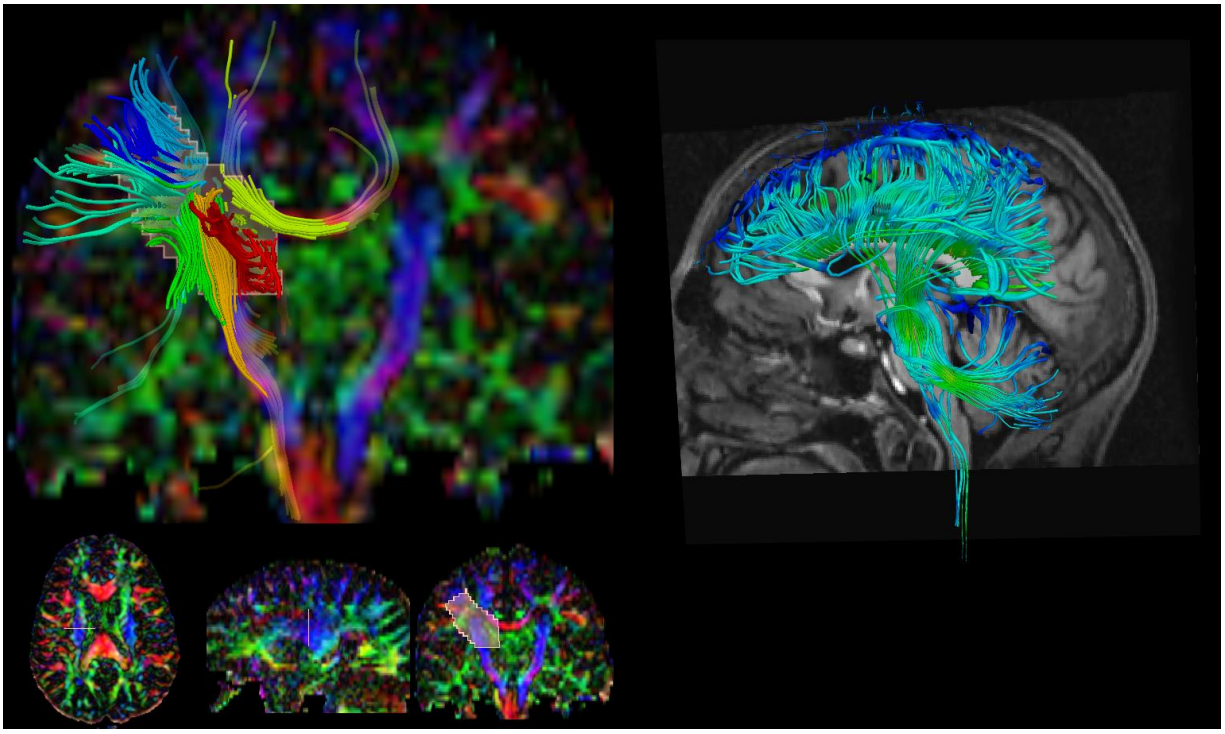

Figure 2-9 Diffusion tensor imaging

2.3.2.2.1 Applications

The principal application is in the imaging of white matter where the location, orientation, and anisotropy of the tracts can be measured. The architecture of the axons in parallel bundles, and their myelin sheaths, facilitate the diffusion of the water molecules preferentially along their main direction. Such preferentially oriented diffusion is called anisotropic diffusion.

The imaging of this property is an extension of diffusion MRI. If a series of diffusion gradients (i.e. magnetic field variations in the MRI magnet) are applied that can determine at least 3 directional vectors (use of 6 different gradients is the minimum and additional gradients improve the accuracy for "off-diagonal" information), it is possible to calculate, for each voxel, a tensor (i.e. a symmetric positive definite 3×3 matrix) that describes the 3-dimensional shape of diffusion. The fiber direction is

indicated by the tensor's main eigenvector. This vector can be color-coded, yielding a cartography of the tracts' position and direction (red for left-right, blue for superior-inferior, and green for anterior-posterior). The brightness is weighted by the fractional anisotropy which is a scalar measure of the degree of anisotropy in a given voxel. Mean diffusivity (MD) or trace is a scalar measure of the total diffusion within a voxel. These measures are commonly used clinically to localize white matter lesions that do not show up on other forms of clinical MRI.

Diffusion tensor imaging data can be used to perform tractography within white matter. Fiber tracking algorithms can be used to track a fiber along its whole length (e.g. the corticospinal tract, through which the motor information transit from the motor cortex to the spinal cord and the peripheral nerves). Tractography is a useful tool for measuring deficits in white matter, such as in aging. Its estimation of fiber orientation and strength is increasingly accurate, and it has widespread potential implications in the fields of cognitive neuroscience and neurobiology.

Some clinical applications of DTI are in the tract-specific localization of white matter lesions such as trauma and in defining the severity of diffuse traumatic brain injury. In one study, DTI identified blast injuries to cerebral tissue in patients who had normal appearing brains on CT and standard MRI - the study validated the imaging method while also resolving important questions about the mechanisms of diffuse axonal injuries. The localization of tumors in relation to the white matter tracts (infiltration, deflection), has been one of the most important initial applications. In surgical planning for some types of brain tumors, surgery is aided by knowing the proximity and relative position of the corticospinal tract and a tumor.

2.3.2.3 Real-time MRI

Real-time magnetic resonance imaging (MRI) refers to the continuous monitoring ("filming") of moving objects in real time. Because MRI is based on time-consuming scanning of k-space, real-time MRI was possible only with low image quality or low temporal resolution. While many different strategies have been developed over the past two decades, a recent development reported a real-time MRI technique based

on radial FLASH and iterative reconstruction that yields a temporal resolution of 20 to 30 milliseconds for images with an in-plane resolution of 1.5 to 2.0 mm. The new method promises to add important information about diseases of the joints and the heart.

2.3.2.4 *Functional MRI*

Functional magnetic resonance imaging (fMRI) of the brain is a non-invasive way to assess brain function using MRI signal changes associated with functional brain activity by detecting changes in blood flow. This technique relies on the fact that cerebral blood flow (CBF) and neuronal activation are coupled. When an area of the brain is in use, blood flow to that region also increases.

The primary form of fMRI uses the blood-oxygen-level-dependent (BOLD) contrast, discovered by Seiji Ogawa. This is a type of specialized brain and body scan used to map neural activity in the brain or spinal cord of humans or other animals by imaging the change in blood flow (hemodynamic response) related to energy use by brain cells. Since the early 1990s, fMRI has come to dominate brain mapping research because it does not require people to undergo shots, surgery, to ingest substances, or be exposed to radiation. Another method of obtaining contrast is arterial spin labeling.

One of the most important points for fMRI in investigating human brain function rests on the fact that brain function is spatially segregated, i.e. specific functions are localized at various sites. This functional specialization can be identified with fMRI and mapped at high spatial resolution. BOLD-fMRI has been widely used in various fields of brain science to identify areas in the brain as the neural basis of their corresponding mental behaviors.

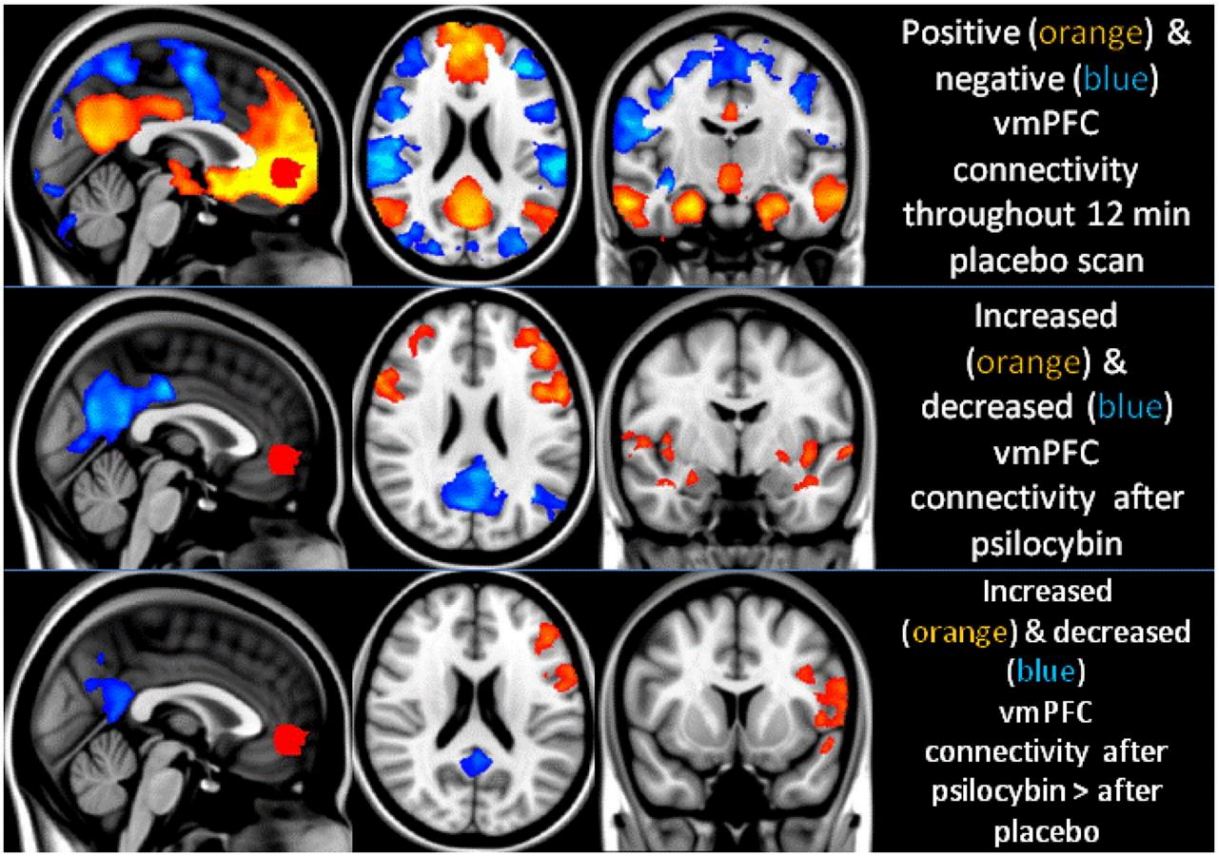

Figure 2-10 Psilocybin-induced changes in vmPFC (red) functional connectivity. (Top) Regions where activity was positively coupled to that of the vmPFC are shown in orange and regions where activity was "negatively" coupled to activity in the vmPFC are shown in blue (it should be noted however, that the appearance of negative connectivity is forced by regression of the global signal). (Middle) Significant increases (orange) and decreases (blue) in functional connectivity after psilocybin infusion. (Bottom) Increases and decreases in functional connectivity after psilocybin that were significantly greater than any connectivity changes after placebo. All analyses were mixed effects, $z > 2.3$, $P < 0.05$ whole-brain cluster corrected, $n = 15$. Note: The significant psycho-physiological interactions in the posterior PCC and left lateral parietal region suggest that the positive coupling (under placebo) has decreased significantly. This finding should not necessarily be interpreted as a negative coupling, simply a significant decrease in a positive coupling.

A single voxel's response signal over time is called its timecourse. Typically, the unwanted signal called the noise, from the scanner, random brain activity and similar elements, is as big as the signal itself. To eliminate these, fMRI studies repeat a stimulus presentation multiple times. The resulting brain activation can be presented graphically by color-coding the strength of activation across the brain or the specific region studied. The technique can localize activity to within millimeters but, using standard techniques, no better than within a window of a few seconds.

2.3.2.4.1 BOLD

The procedure is similar to MRI but uses the change in magnetization between oxygen-rich and oxygen-poor blood as its basic measure.

More specifically, when neurons go active, getting them back to their original (polarized) state requires actively pumping ions back and forth across the neuronal cell membranes. The energy for these motor pumps is produced from glucose. More blood flows in to transport more glucose, also bringing in more oxygen in the form of oxygenated hemoglobin molecules in red blood cells. This is from both a higher rate of blood flow and an expansion of blood vessels. The blood-flow change is localized to within 2 or 3 mm of where the neural activity is. Usually the brought-in oxygen is more than the oxygen consumed in burning glucose, and this causes a net decrease in dHb in that brain area's blood vessels. This changes the magnetic property of the blood, making it interfere less with the magnetization and its eventual decay induced by the MRI process.

The cerebral blood flow (CBF) corresponds differently to the consumed glucose in different brain regions. Initial results show there is more inflow than consumption of glucose in regions such as the amygdala, basal ganglia, thalamus and cingulate cortex, all of which are recruited for fast responses. In regions that are more deliberative, such as the lateral frontal and lateral parietal lobes, it seems that incoming flow is less than consumption. This affects BOLD sensitivity.

Hemoglobin differs in how it responds to magnetic fields, depending on whether it has a bound oxygen molecule. The dHb molecule is more attracted to magnetic fields. Hence, it distorts the surrounding magnetic field induced by an MRI scanner, causing the nuclei there to lose magnetization faster via the T_2^* decay. Thus MR pulse sequences sensitive to T_2^* show more MR signal where blood is highly oxygenated and less where it is not. This effect increases with the square of the strength of the

magnetic field. The fMRI signal hence needs both a strong (1.5 T or higher) magnetic field and a pulse sequence such as EPI, which is sensitive to T_2^* contrast.

The physiological blood-flow response largely decides how well we can measure when neurons are active, namely the temporal sensitivity. The basic time resolution parameter is the TR, which dictates how often a particular brain slice is excited and allowed to lose its magnetization. TRs could vary from the very short (500 ms) to the very long (3 s). For fMRI specifically, the hemodynamic response lasts over 10 seconds, rising multiplicatively (that is, as a proportion of current value), peaking at 4 to 6 seconds, and then falling multiplicatively. Changes in the blood-flow system, the vascular system, integrate responses to neuronal activity over time. Because this response is a smooth continuous function, sampling with ever-faster TRs does not help; it just gives more points on the response curve obtainable by simple linear interpolation anyway. Experimental paradigms such as staggering when a stimulus is presented at various trials can improve temporal resolution, but reduces the number of effective data points obtained.

2.3.2.4.1.1 BOLD signals

The change in the MR signal from neuronal activity is called the hemodynamic response (HDR). It lags the neuronal events triggering it by 1 to 2 seconds, since it takes that long for the vascular system to respond to the brain's need for glucose. From this point it typically rises to a peak at about 5 seconds after the stimulus. If the neurons keep firing, say from a continuous stimulus, the peak spreads to a flat plateau while the neurons stay active. After activity stops, the BOLD signal falls below the original level, the baseline, a phenomenon called the undershoot. Over time the signal recovers to the baseline.

The neuronal processes causing BOLD signal changes are associated with synaptic inputs at the site of activation, not with the output level of firing of the neuron receiving synaptic inputs (Logothetis et al 2001). This means that fMRI reflects the synaptic activity driving neuronal assemblies, but cannot disclose the information content of the neuronal firing patterns produced by the neurons.

The coupling to synaptic activity is very tight. It is obvious that the metabolic load change is coupled directly to the neuronal activation. Furthermore, the vascular response is also coupled very tightly. One of those coupling mechanisms involves glutamate released for synaptic activation, which induces a change in Ca++ in neighboring astrocytes. This results in the release of blood vessel dilators (at the contact point of astrocyte to arterioles and through rapidly diffusible substances like Nitric Oxide) and an increase in CBF.

Such tight coupling of BOLD signal to synaptic activity allows us to use the fMRI signal to probe functional responses in the brain, even though the response time of the BOLD signal (or any other signals based on vascular changes) is over several seconds and much slower than the underlying neuronal processes.

The positive BOLD signal change has been shown to correspond to excitatory activation. An associated increase in the field potential or the appearance of evoked potentials has been observed at the sites where positive BOLD changes are marked. For the positive BOLD, local neuronal activities at the site of activation are responsible.

In addition to the positive and localized BOLD signal, there are areas that show negative BOLD although their magnitude is in general relatively small. There are several possible explanations for this. A likely candidate is a decrease or suppression of local synaptic activity relative to a control state.

2.3.2.4.1.2 Spatial resolution

Spatial resolution of an fMRI study refers to how well it discriminates between nearby locations. It is measured by the size of voxels, as in MRI. A voxel is a three-dimensional rectangular cuboid, whose dimensions are set by the slice thickness, the area of a slice, and the grid imposed on the slice by the scanning process. Full-brain studies use larger voxels, while those that focus on specific regions of interest typically use smaller sizes. Sizes range from 4 to 5 mm to 1 mm. Smaller voxels contain fewer neurons on average, incorporate less blood flow, and hence have less

signal than larger voxels. Smaller voxels also take longer to scan, since scanning time directly rises with the number of voxels per slice and the number of slices. A voxel typically contains a few million neurons and tens of billions of synapses, with the actual number depending on voxel size and the area of the brain being imaged.

The vascular arterial system supplying fresh blood branches into smaller and smaller vessels as it enters the brain surface and within-brain regions, culminating in a connected capillary bed within the brain. The drainage system, similarly, merges into larger and larger veins as it carries away oxygen-depleted blood. The dHb contribution to the fMRI signal is from both the capillaries near the area of activity and larger draining veins that may be farther away. For good spatial resolution, the signal from the large veins needs to be suppressed, since it does not correspond to the area where the neural activity is. This can be achieved either by using strong static magnetic fields or by using spin-echo pulse sequences. With these, fMRI can examine a spatial range from millimeters to centimeters.

2.3.2.4.1.3 Temporal resolution

Temporal resolution is the smallest time period of neural activity reliably separated out by fMRI. One element deciding this is the sampling time, the TR. Below a TR of 1 or 2 seconds, however, scanning just generates sharper HDR curves, without adding much information beyond what mathematically filling in the gaps of the curve produced by a higher TR would. Temporal resolution can be improved by staggering stimulus presentation across trials. If one-third of data trials are sampled normally, one-third at 1 s, 4 s, 7 s and so on, and the last third at 2 s, 5 s and 8 s, the combined data provide a resolution of 1 s, though with only one-third as many total events.

The time resolution needed depends on brain processing time for various events. An example of the broad range here is given by the visual processing system. What the eye sees is registered on the photoreceptors of the retina within a millisecond or so. These signals get to the primary visual cortex via the thalamus in tens of milliseconds. Neuronal activity related to the act of seeing lasts for more than 100 ms. A fast reaction, such as swerving to avoid a car crash, takes around 200 ms. By about half-

a-second, awareness and reflection of the incident sets in. Remembering a similar event may take a few seconds, and emotional or physiological changes such as fear arousal may last minutes or hours. Learned changes, such as recognizing faces or scenes, may last days, months, or forever. Most fMRI experiments study brain processes lasting a few seconds, with the study conducted over some tens of minutes. Subjects may move their heads during that time, and this head motion needs to be corrected for. So does drift in the baseline signal over time. Boredom and learning may modify both subject behavior and cognitive processes.

2.3.2.4.1.4 Translating BOLD signal to neural activation

The BOLD contrast reflects mainly the inputs to a neuron and the neuron's integrative processing within its body, and less the output firing of neurons.

However, the BOLD signal cannot separate feedback and feedforward active networks in a region; the slowness of the vascular response means the final signal is the summed version of the whole region's network; blood flow is not in spurts as the processing proceeds. Also, both inhibitory and excitatory input to a neuron from other neurons sum and contribute to the BOLD signal. Within a neuron they might cancel out. The BOLD response can also be affected by a variety of factors, including disease, sedation, anxiety, medications that dilate blood vessels, and attention (neuromodulation).

The amplitude of the BOLD signal does not necessarily affect its shape. A higher-amplitude signal may be seen for stronger neural activity, but peaking at the same place as a weaker signal. Also, the amplitude does not necessarily reflect behavioral performance. A complex cognitive task may initially trigger high-amplitude signals associated with good performance, but as the subject gets better at it, the amplitude may come down with performance staying the same. This is expected to be from the brain more efficiently marshaling neurons to perform the task, decreasing wasteful energy expenditure. The BOLD response across brain regions cannot be compared directly even for the same task, since the density of neurons and the blood-supply

characteristics are not constant across the brain. However, the BOLD response can often be compared across subjects for the same brain region and the same task.

2.3.2.4.1.5 Sources of noise

The BOLD signature of activation is relatively weak, however, so other sources of noise in the acquired data must be carefully controlled. This means that a series of processing steps must be performed on the acquired images before the actual statistical search for task-related activation can begin.

Noise is unwanted changes to the MR signal from elements not of interest to the study. The five main sources of noise in fMRI are thermal noise, system noise, physiological noise, random neural activity and differences in both mental strategies and behavior across people and across tasks within a person. Thermal noise multiplies in line with the static field strength, but physiological noise multiplies as the square of the field strength. Since the signal also multiplies as the square of the field strength, and since physiological noise is a large proportion of total noise, higher field strengths above 3 T do not always produce proportionately better images.

Heat causes electrons to move around and distort the current in the fMRI detector, producing thermal noise. Thermal noise rises with the temperature. It also depends on the range of frequencies detected by the receiver coil and its electrical resistance. It affects all voxels similarly, independent of anatomy.

System noise is from the imaging hardware. One form is scanner drift, caused by the superconducting magnet's field drifting over time. Another form is changes in the current or voltage distribution of the brain itself inducing changes in the receiver coil and reducing its sensitivity. A procedure called impedance matching is used to bypass this inductance effect. There could also be noise from the magnetic field not being uniform. This is often adjusted for by using shimming coils, small magnets physically inserted, say into the subject's mouth, to patch the magnetic field. The nonuniformities are often near brain sinuses such as the ear and plugging the cavity for long periods can be discomfiting. The scanning process acquires the MR signal in

k-space, in which overlapping spatial frequencies (that is repeated edges in the sample's volume) are each represented with lines. Transforming this into voxels introduces some loss and distortions.

Physiological noise is from head and brain movement in the scanner from breathing, heart beats, or the subject fidgeting, tensing, or making physical responses such as button presses. Head movements cause the voxel-to-neurons mapping to change while scanning is in progress. Since fMRI is acquired in slices, after movement, a voxel continues to refer to the same absolute location in space while the neurons underneath it would have changed. Another source of physiological noise is the change in the rate of blood flow, blood volume, and use of oxygen over time. This last component contributes to two-thirds of physiological noise, which, in turn, is the main contributor to total noise.

Even with the best experimental design, it is not possible to control and constrain all other background stimuli impinging on a subject—scanner noise, random thoughts, physical sensations, and the like. These produce neural activity independent of the experimental manipulation. These are not amenable to mathematical modeling and have to be controlled by the study design.

A person's strategies to respond or react to a stimulus, and to solve problems, often change over time and over tasks. This generates variations in neural activity from trial to trial within a subject. Across people too neural activity differs for similar reasons. Researchers often conduct pilot studies to see how participants typically perform for the task under consideration. They also often train subjects how to respond or react in a trial training session prior to the scanning one.

2.3.2.4.2 Non-BOLD

To overcome the disadvantage of BOLD signal, various non-invasive measurements have been developed. CBF and CBV measurements, both of which are based on the vascular response have better specificity for localizing functional activity in capillaries or functional activity linked blood volume change. Both show the response time to be

shorter than BOLD signal by about a second, which corresponds to the transit time of the blood from arterial side to venous side of the capillary bed.

Recently, it has been shown that MRI signals, with an application of strong field gradients as in water diffusion measurement, responds to neuronal activation and the signal change has good spatial specificity (Le Bihan 2006). This response appears to reflect a change in the apparent diffusion constant of water in the tissue. It could be interpreted in terms of cellular swelling caused by evoked neural activity. This phenomenon is interesting but more study is needed to establish the mechanism of this signal change and its characteristics.

It has been an ambition of many people to detect electro-magnetic events caused by neural activity directly using MRI. Such direct detection of current induced local magnetic field or ion movements would provide the means to study neuronal events at high spatial and temporal resolution. Despite active efforts with many experiments using in vitro or model systems, the in vivo detection of electrical events still eludes MR spectroscopists.

2.4 Magnetoencephalogram (MEG)

The magnetoencephalogram (MEG) is a record of magnetic fields, measured outside the head, produced by electrical activity within the brain. Typically MEG sensors are housed in a helmet shaped container in which the subject places their head during the measurement process. The magnetic fields are produced by the same underlying electrical changes that give rise to the EEG that is they are due mainly to post-synaptic currents flowing across pyramidal neurons. Unlike the electroencephalogram however the magnetic fields outside the head are hardly affected by the conductivity of the tissues within the head. Accurate reconstruction of the neuronal activity that produced the external magnetic fields therefore requires simpler models than with EEG. The high spatial and temporal resolution with which brain activity can be measured can be used to reveal how groups of neurons communicate and has important clinical applications.

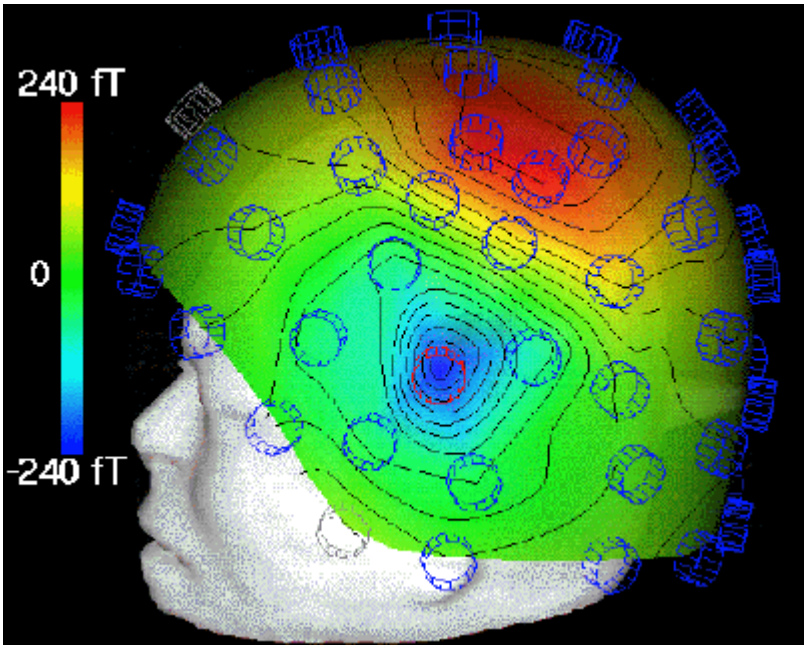

Figure 2-11 Magnetoencephalography (MEG) sensor array for detecting sources of electrical activity within the brain. The contours correspond to the magnitude of the field induced by the source. (Source: CTF Systems Inc.)

The magnetic fields outside the head due to electrical activity within the brain are in the hundreds of femto (10-15) Tesla, that is approximately 100 million time smaller than the earth's magnetic field. Although the first Magnetoencephalogram was based on a million turn coil (Cohen et al. 1968), modern systems rely on the superconducting quantum interference device or SQUID (Clarke 1994) for sensitivity. These devices convert the sub-quanta changes in magnetic flux into voltage changes. Typically the SQUIDs are coupled to superconducting coils or flux transformers which are situated as close as possible to the subject's head (within 2cm typically). Magnetic field changes in the flux transformers cause a change in superconducting current in the transformer coils that is passed via an input coil to the SQUID itself. The ability to measure such small fields also makes the devices very sensitive to other magnetic field changes in the environment. For example a car at 2km distance would cause a similar change in magnetic flux to that due to brain activity (Weinstock 1996). For this reason, MEG systems are typically housed in magnetically shielded rooms. These rooms are often composed of a number of layers of materials with different magnetic properties.

The next major problem is to separate the brain signal from the external noise. An array of reference channels can be used to compensate for the effects of imbalance, and to noise signals, by subtracting a weighted sum of the reference sensor signals from each signal sensor. The reference sensors are placed in such way that they are least sensitive to the signals of interest, and so contain mostly a record of external noise sources.

2.4.1 The inverse problem

The challenge posed by MEG is to determine the location of electric activity within the brain from the induced magnetic fields outside the head. Problems such as this, where model parameters (the location of the activity) have to be estimated from measured data (the SQUID signals) are referred to as inverse problems (in contrast to forward problems where the model parameters (e.g. source location) are known and the data (e.g. the field at a given distance) is to be estimated.) The primary difficulty is that the inverse problem does not have a unique solution (i.e., there are infinite possible "correct" answers), and the problem of defining the "best" solution is itself the subject of intensive research. Possible solutions can be derived using models involving prior knowledge of brain activity.

2.4.1.1 Dipole fitting

Often the underlying assumption is that only one region of cortex is strongly time-locked to an external stimulus. By averaging the brain responses across many presentations of that stimulus the signals due to all other non time-locked sources are attenuated. One can model the electrical activity using a simple dipole model and, in order to estimate the exact location of the active piece of cortex, move it around the brain until the magnetic field it produces matches the measured magnetic field. One can do this for a number of time points or time ranges and for more complex dipole models. The disadvantages are that the methods are generally poorly suited to characterising responses that do not average very well, such as responses related to higher cognitive functions. Moreover, the more dipoles one incorporates the less stable the fits become.

2.4.1.2 *Minimum norm based approaches*

If one assumes that many electrical sources are active across the cortical sheet at any one time then the number of parameters that need to be estimated are larger than the number of measurements. Additional constraints are therefore needed to obtain a unique solution. With the traditional minimum norm method this is achieved by assuming that out of all source configurations that can explain the measured data, the one that has the minimum overall source power is the optimum one. Or in other words, it assumes that the brain is efficient in terms of its energy use. However using this single assumption results in electrical source estimates that are entirely superficial (as deeper sources would need to have larger amplitude to have the same impact on the sensors), although this can be overcome by depth/noise weighting.

3 Blind Signal Processing (BSP)

The term Blind Signal Processing, refers to a wide class of highly underdetermined problems in signal and image processing, where one needs to extract the underlying sources or the system parameters from a set of mixtures. The blind signal processing techniques principally do not use any training data and do not assume a priori knowledge about parameters of convolutive, filtering and mixing systems, hence the name blind.

There are many different blind source separation methods according to the assumptions made about the sources, the filter and the additive noise. Briefly, sources may be one-dimensional (e.g. acoustic signals), two-dimensional (images) or three-dimensional (volumetric data), may be statistically independent, may have different second order spectra, may be stationary or cyclostationary, may be non-Gaussian, while in other cases they are considered independent and identically distributed. The mixing can be linear, or nonlinear on one hand, and instantaneous (also known as memoryless) or convolutive.

Due to the underdetermination of the problem, methods for blind source separation generally seek to narrow the set of possible solutions in a way that is unlikely to exclude the desired solution. The basic hypothesis of the system is that in the most of cases it is modeled as a linear time invariant filter, while the assumptions for the additive noise describe a Gaussian or non-Gaussian noise, a temporally white noise, a spectrally uncorrelated noise, or a spectrally correlated noise with known spatial coherence.

Regardless of the specific system type, blind signal processing includes three major areas, depending on whether we desire to extract the input signals or the system parameters: Blind Signal Separation and Extraction, Independent Component Analysis (ICA), and Blind Multichannel Blind Deconvolution and Equalization.

In **blind source extraction**, our goal is to recover the source(s) given the observation signal. If there are more than one sources the problem is called Blind Source Separation (BSS). In the case of BSS the linear system may be either instantaneous or convolutive (general MIMO). In the case of Blind Deconvolution (BD) we want to invert a linear filter which, of course, operates on its input via the convolution operator, hence the name “de-convolution” attributed to this problem.

The source separation/extraction problem has an inherent ambiguity in the order and the scale of the sources: the original signals cannot be retrieved in their original order or scale unless some further information is available.

In **blind system identification**, our goal is to obtain the system parameters rather than recovering the source signals. If the system is memoryless then our goal is to recover the mixing matrix. If the system involves non-trivial convolution then the goal is to extract the filter taps.

3.1 The linear BSS problem

In a typical scenario of an instantaneous linear BSS problem, real signals $s_{\mathrm{i}}(t)$ from N sources are recorded by M sensors; t is a multi-index and refers to data of any dimension. The sensor signals $x_{\mathrm{i}}(t)$ are instantaneous linear combinations of the source signals, and are possibly contaminated by additive sensor noise $\xi_{\mathrm{i}}(t)$:

$$\begin{aligned} x_1(t) &= a_{1,1}s_1(t) + \cdots + a_{1,N}s_N(t) + \xi_1(t) \\ &\vdots \qquad\quad \vdots \qquad\qquad \vdots \\ x_M(t) &= a_{M,1}s_1(t) + \cdots + a_{M,N}s_N(t) + \xi_M(t) \end{aligned} \tag{1}$$

where $a_{i,i}$ are the mixing coefficients. In matrix notation, the linear BSS problem has the form

$$x(t) = As(t) + \xi(t) \tag{2}$$

where $s(t)$, $x(t)$ and $\xi(t)$ are column vectors with values $s_i(t)$, $x_i(t)$ and $\xi_i(t)$, respectively.

The BSS problem consists of finding an estimate $Y(X)$ of S, given only the observed (possibly noisy) data X. If no a priori information is available, the latter is possible up to an arbitrary permutation and scaling only. In a particular case when the matrix A is square (i.e. $N = M$) and invertible, and under the assumption of zero noise, the problem is equivalent to estimating the unmixing matrix

$$W = [w_1, \cdots, w_N]^T = EA^{-1} \tag{3}$$

such that

$$EY = WX \tag{4}$$

where E is a permutation and scaling matrix.

In the following pages, different methods and techniques applied in BSP are described. A detailed description of each technique is beyond the scope of this study and the reader is referred to the cited works.

3.2 Principal component analysis

Principal component analysis (PCA) and the closely related Karhunen-Loève transform, or the Hotelling transform, are classic techniques in statistical data analysis, feature extraction, and data compression, stemming from the early work of Pearson (Pearson, 1901) and later proposed by Hotelling (Hotelling, 1933). Given a set of multivariate measurements, the purpose is to find a smaller set of variables with

less redundancy that would give as good a representation as possible (Hyvärinen et al. 2001).

The central idea of PCA is to reduce the dimensionality of a data set consisting of a large number of interrelated variables, while retaining as much as possible of the variation present in the data set. This is achieved by transforming to a new set of variables, the principal components (PCs), which are uncorrelated, and which are ordered so that the first few retain most of the variation present in all of the original variables.

Briefly, PCA is an orthogonal linear transformation that transforms a set of observations of possibly correlated variables, to a new coordinate system such that the greatest variance by any projection of the data comes to lie on the first coordinate (called the first principal component), the second greatest variance on the second coordinate, and so on (Jolliffe, 2002). The number of principal components is less than or equal to the number of original variables and each succeeding component in turn has the highest variance possible under the constraint that it be orthogonal to (i.e., uncorrelated with) the preceding components. Principal components are guaranteed to be independent only if the data set is jointly normally distributed. PCA is sensitive to the relative scaling of the original variables.

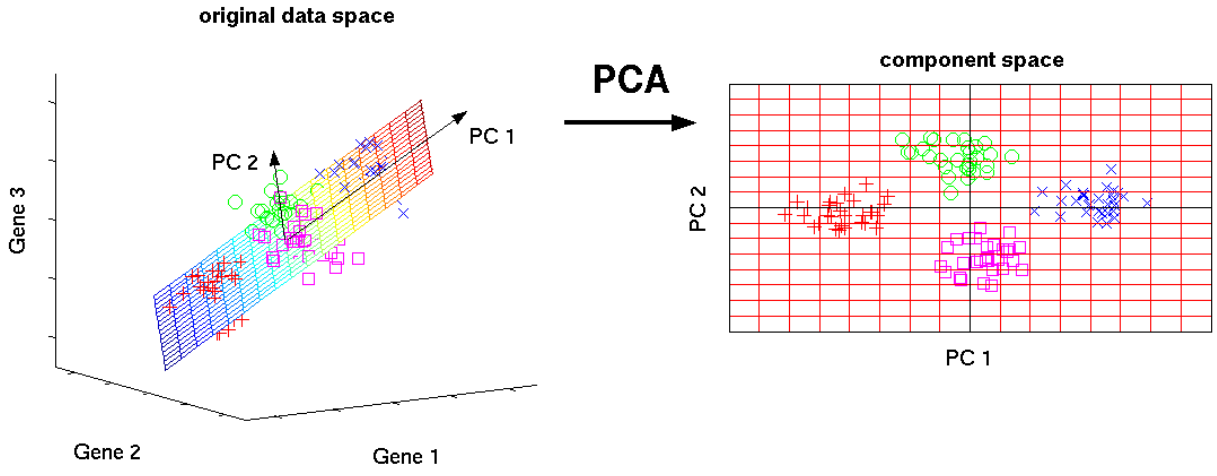

Figure 3-1 Illustrated are three-dimensional gene expression data which are mainly located within a two-dimensional subspace. PCA is used to visualize these data by reducing the dimensionality of the data: The three original variables (genes) are reduced to a lower number of two new variables termed principal

components (PCs). Left: Using PCA, we can identify the two-dimensional plane that optimally describes the highest variance of the data. This two-dimensional subspace can then be rotated and presented as a two-dimensional component space (right). Reproduced by Matthias Scholz, 2006.

Mean subtraction (a.k.a. "mean centering") is necessary for performing PCA to ensure that the first principal component describes the direction of maximum variance. If mean subtraction is not performed, the first principal component might instead correspond more or less to the mean of the data. A mean of zero is needed for finding a basis that minimizes the mean square error of the approximation of the data (Miranda et al, 2008).

For more detailed description of the methods and variations of PCA, the reader is referred to recent books on the subject (Diamantaras, Kung, 1996; Hyvärinen et al, 2001; Jolliffe, 2002) that provide extensive discussion on related problems and methods.

3.3 Independent Component Analysis

Independent component analysis (ICA) is a statistical and computational technique for revealing hidden factors that underlie sets of random variables, measurements, or signals.

ICA defines a generative model for the observed multivariate data, which is typically given as a large database of samples. In the model, the data variables are assumed to be linear mixtures of some unknown latent variables, and the mixing system is also unknown. The latent variables are assumed non-Gaussian and mutually independent, and they are called the independent components of the observed data. These independent components, also called sources or factors, can be found by ICA.

The data analyzed by ICA could originate from many different kinds of application fields, including digital images, document databases, economic indicators and psychometric measurements. In many cases, the measurements are given as a set of parallel signals or time series. Typical examples are mixtures of simultaneous speech

signals that have been picked up by several microphones (usually referred as cocktail party problem), brain waves recorded by multiple sensors, interfering radio signals arriving at a mobile phone, or parallel time series obtained from some industrial process.

ICA finds the independent components by maximizing the statistical independence of the estimated components. There are many ways to define independence, and this choice governs the form of the ICA algorithm. The two broadest definitions of independence for ICA are Minimization of mutual information (MMI) and Maximization of non-Gaussianity.

Typical algorithms for ICA use centering, whitening, and dimensionality reduction as preprocessing steps in order to simplify and reduce the complexity of the problem for the actual iterative algorithm. Whitening and dimension reduction can be achieved with PCA or singular value decomposition. Whitening ensures that all dimensions are treated equally a priori before the algorithm is run. Many well-known algorithms for ICA like Infomax, FastICA and JADE amongst others are described in the following sections.

Comparison of ICA and PCA

The "cocktail party effect" with 2 microphones and 2 people talking illustrates this concept well. If two microphones are placed in two different places in the room, they will each record a particular linear combination of the two voices. If Gaussianity was assumed, we could perform PCA or a Factorial Analysis to the recordings to identify the voice of each speaker. The resulting components would be two new orderly voice combinations (Figure 3-2a). Therefore, such a technique fails to isolate each speaker’s voice. On the other hand, if non-Gaussianity is assumed, then ICA could be applied to the same problem and the result would be quite different. ICA is able to distinguish the voice of each speaker from the linear combination of their voices (Figure 3-2b). This reasoning can be applied to many biological recording involving

multiple source signals (e.g. EEG). However, there are two main differences in the interpretation of extracted components using ICA instead of PCA. First, in ICA, there is no order of magnitude associated with each component. In other words, there is no better or worst components (unless the user decides to order them following his own criteria). Second, the extracted components are invariant to the sign of the sources.

a)

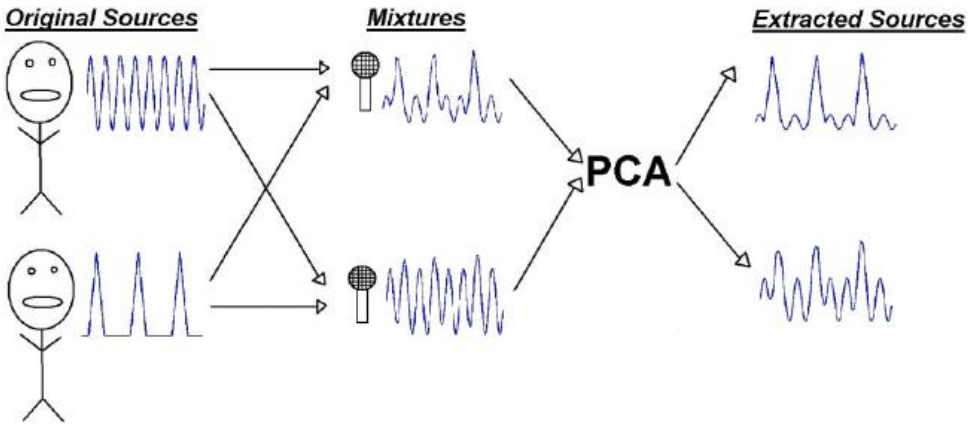

b)

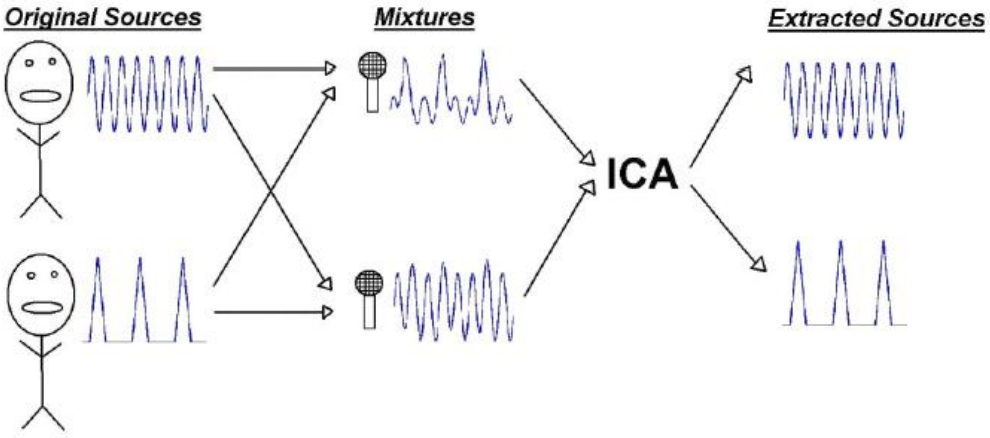

Figure 3-2 Comparison between PCA (a) and ICA (b) in the context of the "cocktail party effect".

3.3.1 Basic System

The data is represented by the random vector x and the components as the random vector s

$$x(k) = [x_1(k), \cdots, x_m(k)]^T$$

$$s(k) = [s_1(k), \cdots, s_n(k)]^T$$

(5)

The task is to transform the observed data x using a linear static transformation W

$$s = Wx$$

(6)

into maximally independent components measured by some function F of independence.

$$F(s_1, \cdots, s_n)$$

(7)

3.3.1.1 Linear noiseless ICA

The components x_i of the observed random vector $x = [x_1, \cdots, x_m]^T$ are generated as a sum of the independent components $s_\mathrm{k}, k = 1, \cdots, n$:

$$x_\mathrm{i} = a_{\mathrm{i,1}} s_1 + \cdots + a_{\mathrm{i,k}} s_\mathrm{k} + \cdots a_{\mathrm{i,n}} s_n$$

(8)

weighted by the mixing weights $a_{\mathrm{i,k}}$. The same generative model can be written in vectorial form as:

$$x = \sum_{k=1}^{n} s_k a_k$$

(9)

where the observed random vector x is represented by the basis vectors

$$a_k = \left[a_{1,k}, \cdots, a_{m,k}\right]^T$$

(10)

The basis vectors a_k form the columns of the mixing matrix A and the generative formula can be written as

$$A = [a_{1,}, \cdots, a_n]$$

$$x = As$$

(11)

where

$$s = [s_1, \cdots, s_n]^T$$

(12)

Given the model and realizations (samples) $x_1, \cdots, x_N$ of the random vector x, the task is to estimate both the mixing matrix A and the sources s. This is done by adaptively calculating the ω vectors and setting up a cost function which either maximizes the nongaussianity of the calculated

$$s_k = (\omega^T * x)$$

(13)

or minimizes the mutual information. In some cases, a priori knowledge of the probability distributions of the sources can be used in the cost function.

The original sources s can be recovered by multiplying the observed signals x with the inverse of the mixing matrix $= A^{-1}$, also known as the unmixing matrix. Here it is assumed that the mixing matrix is square ($n = m$). If the number of basis vectors is

greater than the dimensionality of the observed vectors, $n > m$, the task is overcomplete but is still solvable with the pseudo inverse.

3.3.1.2 Linear noisy ICA

With the added assumption of zero-mean and uncorrelated Gaussian noise n, the ICA model takes the form

$$x = As + n \quad (14)$$

3.3.1.3 Nonlinear ICA

The mixing of the sources does not need to be linear. Using a nonlinear mixing function $f(\cdot|\theta)$ with parameters θ the nonlinear ICA model is

$$x = f(\mathrm{s}|\theta) + n \quad (15)$$

3.3.2 Fast ICA

FastICA is a stochastic method that uses a fixed-point iterative approach to extract maximally non-Gaussian sources. The independence criterion adopted can be higher order statistics or the negentropy of the output (Hyvärinen and Oja, 2000). Two approaches exist: The symmetric approach estimates all the ICs in parallel and the deflationary approach estimates the ICs one at a time.

The entire FastICA algorithm can be summarised as follows:

Step 1 Center the data x, by computing the mean of each component of x and subtracting that mean. This has the effect of making each component have zero mean.

Step 2 Whiten the data to give x so that the new components are uncorrelated and have variance one by using eigenvalue decomposition of the covariance matrix of the data.

Single component extraction

The iterative algorithm finds the direction for the weight vector W maximizing the non-Gaussianity of the projection $W^T X$ for the data x. The function $g(u)$ is the derivative of a nonquadratic nonlinearity function $G(u)$. Good equations for G (shown with their derivatives g and second derivatives g') are:

$$G(u) = log\cosh(u);\ g(u) = \tanh(u);\ \ g'(u) = 1 - \tanh^2(u) \tag{16}$$

$$G(u) = -e^{-u^2/2};\ g(u) = ue^{-u^2/2};\ \ g'(u) = (1-u^2)e^{-u^2/2} \tag{17}$$

Step 3 Select the initial value of random weight vector W;

Step 4 Select non-quadratic function G; Eq. (16) is a good general-purpose equation, while Eq. (17) is highly robust.

Step 5 Let

$$W \leftarrow E\{xg(W^T x)\} - E\{g'(W^T x)\}W \tag{18}$$

Step 6 Repeat the iteration until the algorithm converges.

For the estimation of multiple independent components, the method of maximizing non-Gaussian Property must be extended. Corresponding to different independent components, W_i should be orthogonal in the whitening space and the deflationary orthogonalisation method and symmetric orthogonalisation method can be adopted.

On simulated data, this algorithm does better in terms of spatial correlation of the estimated sources with the original sources, for super-Gaussian sources when compared to the other sources. For smaller number of components, FastICA with the gauss non-linearity provides better performance compared to the other two non-linearities for the Gaussian and sub-Gaussian sources. However, for a slightly larger simulated set, all three non-linearities result in very similar performance. Overall, the

general performance of FastICA using $tanh$ is better than the results obtained using the other two non-linearities.

The fixed-point algorithm and the underlying contrast functions have a number of desirable properties when compared with other methods for ICA (Hyvärinen, 1999).

- The convergence is cubic (or at least quadratic), under the assumption of the ICA data model. This is in contrast to gradient descent methods, where the convergence is only linear. This means a very fast convergence, as has been confirmed by simulations and experiments on real data.
- Contrary to gradient-based algorithms, there are no step size parameters to choose (in the original fixed-point algorithm). This means that the algorithm is easy to use. Even in the stabilized version, reasonable values for the step size parameter are very easy to choose.
- The algorithm finds directly independent components of (practically) any non-Gaussian distribution using any nonlinearity g. This is in contrast to many algorithms, where some estimate of the probability distribution function has to be first available, and the nonlinearity must be chosen accordingly.
- The performance of the method can be optimized by choosing a suitable nonlinearity g. In particular, one can obtain algorithms that are robust and/or of minimum variance.
- The independent components can be estimated one by one, which is roughly equivalent to doing projection pursuit.
- The fixed-point algorithm inherits most of the advantages of neural algorithms: It is parallel, distributed, computationally simple, and requires little memory space. Stochastic gradient methods seem to be preferable only if fast adaptivity in a changing environment is required.

3.3.3 JADE OPAC

JADEOPAC (joint approximate diagonalization of eigenmatrices) is a deterministic algorithm which diagonalizes fourth order cumulant matrices using the Jacobi technique to obtain spatially independent sources (Cardoso and Souloumiac, 1993).

Joint approximate diagonalization of eigenmatrices (JADE) refers to one principle of solving the problem of equal eigenvalues of the cumulant tensor. In this algorithm, the tensor EVD is considered more as a preprocessing step. Eigenvalue decomposition can be viewed as diagonalization. The matrix W diagonalizes $F(M)$ for any M. In other words, $WF(M)W^T$ is diagonal. This is because the matrix F is of a linear combination of terms of the form $w_i w_i^T$, assuming that the ICA model holds.

Thus, we could take a set of different matrices $M_i, i = 1, \dots, k,$, and try to make the matrices $WF(M_i)W^T$ as diagonal as possible. In practice, they cannot be made exactly diagonal because the model does not hold exactly, and there are sampling errors. The diagonality of a matrix can be measured, for example, as the sum of the squares of off-diagonal elements. Equivalently, since an orthogonal matrix W does not change the total sum of squares of a matrix, minimization of the sum of squares of off-diagonal elements is equivalent to the maximization of the sum of squares of diagonal elements.

The basic principle of the JADE algorithm is to take the eigenmatrices of the cumulant tensor as the matrices M_i. This leads to a set of just n matrices that give all the relevant information on the cumulants, in the sense that they span the same subspace as the cumulant tensor (Hyvärinen et al, 2001).

JADE suffers from the same problems as all methods using an explicit tensor EVD. Such algorithms cannot be used in high-dimensional spaces, but in problems of low dimensionality (small scale) JADE offers a competitive alternative. In fact, JADE is fast and the results are comparable to those obtained using Infomax. In the case of transiently task related components this algorithm shows spatial extent of activations to be higher than the obtained using Infomax.

3.3.4 EVD

EVD (eigenvalue decomposition) is based on second order statistics and very similar to AMUSE, the main difference being that EVD uses higher order correlations instead of second order correlations and is based on non-smooth optimization theory. To achieve separation, the source signals are required to have linearly independent higher self-correlation functions of even order. The algorithm does not assume non-Gaussianity, non-stationarity and independence. It creates and sums a set of shifted cross variance matrices, after this it applies singular-value decomposition to achieve source separation. The EVD approach is fast and useful when the spectra of the components are different (Georgiev and Cichocki, 2002).

3.3.5 AMUSE

AMUSE (algorithm for multiple unknown sources extraction) is a second order method based on the EVD algorithm. It utilizes the structure within the data to obtain uncorrelated components. It performs singular value decomposition on the shifted cross-variance matrix and the shift should be chosen such that the autocorrelations of the sources at that shift are non-zero and as different from each other as possible (Tong et al, 1991).

AMUSE is highly dependent on the differentiability of the spectra i.e. the autocorrelation of the sources should be different, for a given delay and its performance suffers greatly when this condition is not met.

3.3.6 SIMBEC

SIMBEC (simultaneous blind extraction using cumulants) is a deterministic algorithm that exploits natural gradient ascent in a Stiefel manifold to simultaneously extract sources using a contrast function based on higher order cumulants with a learning rate that provides fast convergence. (Amari, 1999; Cruces et al., 2001).

For smaller number of components, SIMBEC performs well for the sources of interest. However, SIMBEC may prove useful to identify the sub-Gaussian sources, i.e.

artifacts in fMRI data as its performance for these sources was consistently observed to be very good. SIMBEC is also observed to be one of the faster algorithms.

3.3.7 Infomax

Infomax (Bell & Sejnowski, 1995), is a gradient based neural network algorithm, with a learning rule for information maximization using higher order statistics to maximize the information mapped between input and output of a network. In perfect cases, it does provide the best estimate to ICA components. The strength of this algorithm comes from its direct relationship to information theory and is derived through an information maximization principle. The algorithm favors separation of super-Gaussian sources and t To improve separation of the mixture containing both super-Gaussian and sub-Gaussian sources, Extended Infomax (Lee et al, 1999) can be used.

3.3.8 ERICA

ERICA (equivariant robust ICA) is an algorithm that minimizes the amount of signal and noise interference on the estimated sources. It uses a cumulant based entropy cost function instead of a nonlinearity. The algorithm uses quasi-Newton iterations and converges at a saddle point of the entropy cost function. The algorithm achieves isotropic convergence, is fast and is independent of the source distributions regardless of Gaussian noise. It is also asymptotically equivariant for sufficient number of samples (Cruces et al., 2000).

3.3.9 Constrained ICA

Constrained ICA is a semi-blind ICA algorithm that utilizes prior information about desired sources as reference signals to extract only the desired sources. This algorithm uses fixed point iteration scheme (fICA-R) for optimizing the constrained ICA contrast function. Compared with the Newton-like ICA with reference, the fICA-R algorithm has advantages as it has no learning rate and is insensitive to the initialisation and is relatively simplistic since no second derivatives are needed. The

resulting independent components have higher SNR ratio than traditional ICA algorithms (Lin et al., 2007, 2010).

3.3.10 SOBI - COMBI

COMBI is an algorithm which is the result of a combination of two different methods (Combination and Multi-combination of WASOBI and EFICA). SOBI (second order blind identification) was developed with the aim of dealing with sources which could be temporally correlated. It exploits second order statistic to get rid of temporal correlation and maximize the separability of sources (Belouchrani et al., 1993).

WASOBI is an asymptotically optimal algorithm for autoregressive sources (Yeredor, 2000), while EFICA is an asymptotically efficient version of the FastICA algorithm (Koldovsky et al., 2006).

4 Application on fMRI

ICA allows one to extract or unmix unknown source signals which are linearly mixed together. For fMRI data, temporal and spatial ICA are possible, but spatial ICA is by far the most common approach. ICA has been successfully applied to single subject and single session analyses. Group analysis of fMRI is important to study specific conditions within or between groups of subjects. There are three main stages to Group ICA; Data Compression, ICA, and Back Reconstruction (Calhoun et al., 2001). The outputs from these stages are multiple time courses. Each time course has an image map associated with it.

As a preprocessing step, Principal Components Analysis (PCA) is used as a technique to reduce the dimensions. Two data reduction steps are used for multiple subjects: after each subject's functional data is reduced, the subjects are then concatenated into one group and put through another data reduction step.

For the application of BSS methods on selected biomedical signals, GroupICATv3.0a version of the Group ICA Of fMRI Toolbox was used (Calhoun et al., 2003; Calhoun et al., 2004). It is a MATLAB toolbox which implements multiple algorithms for independent component analysis and blind source separation of group (and single subject) fMRI data (GIFT) and EEG data (EEGIFT). For detailed information regarding the methods and utilities offered by the Toolbox, the reader is referred to the cited material.

An example dataset of 3 participants on a visuomotor paradigm has been used (Calhoun et al., 2001). A small demonstration of the toolbox, a comparison of selected BSS methods and their results will follow. On fMRI, main comparison of IC extraction will be some known brain functional networks, like DMN as shown on Figure 4-1.

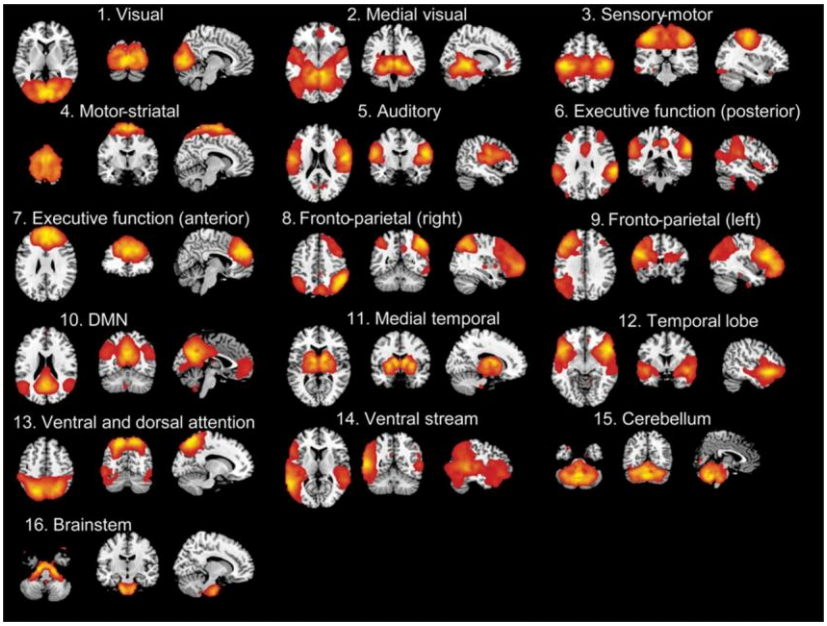

Figure 4-1 Basic functional networks (Shumskaya et al.,2012)

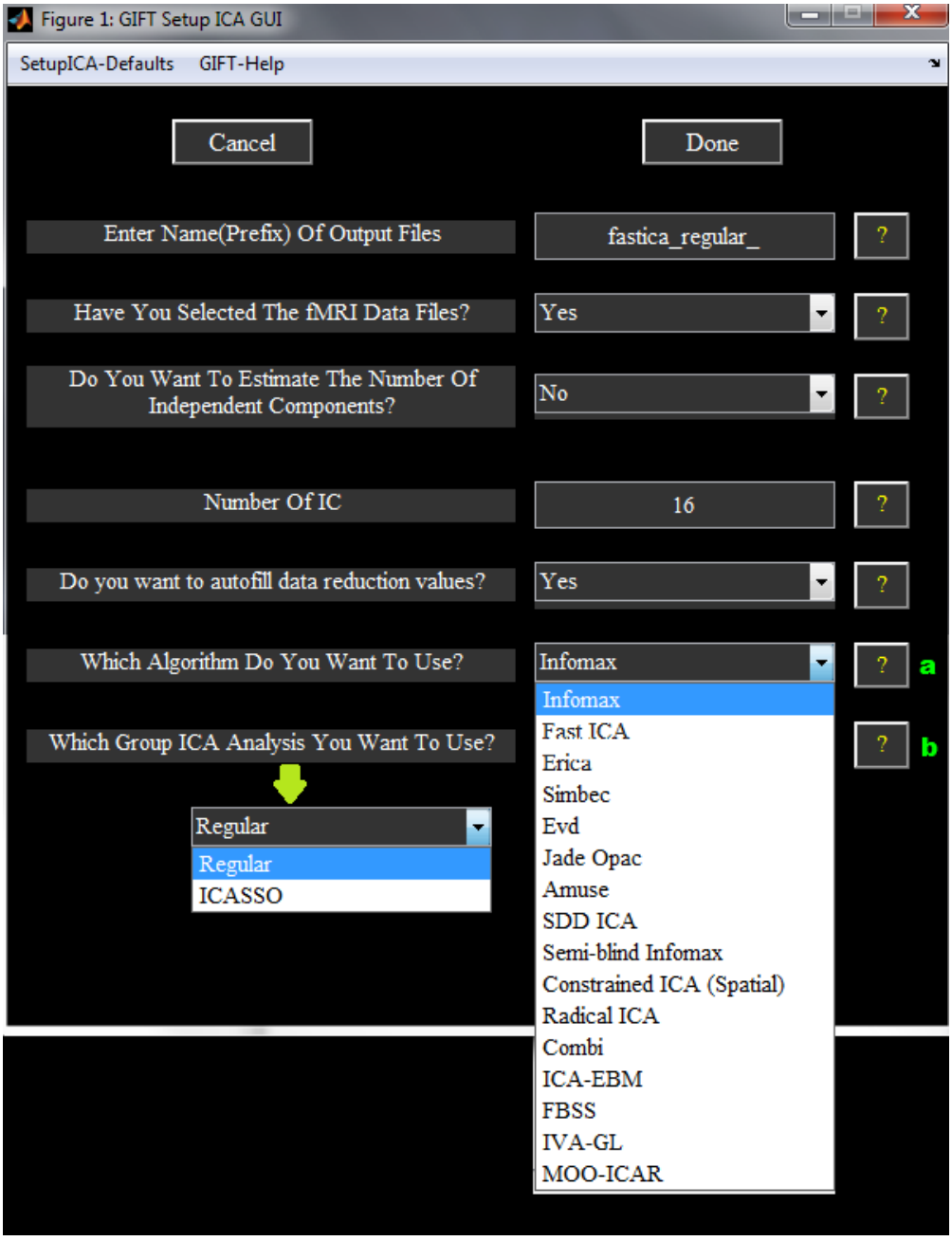

Figure 4-2 GIFT ICA Analysis Setup Options

The available algorithms for ICA analysis include FastICA, Infomax, SIMBEX, JADE, AMUSE amongst others. FastICA was chosen to run on a single-run analysis and a multiple-run (ICASSO) that determines the reliability of the components and the stability of the method and Infomax on multi-run.

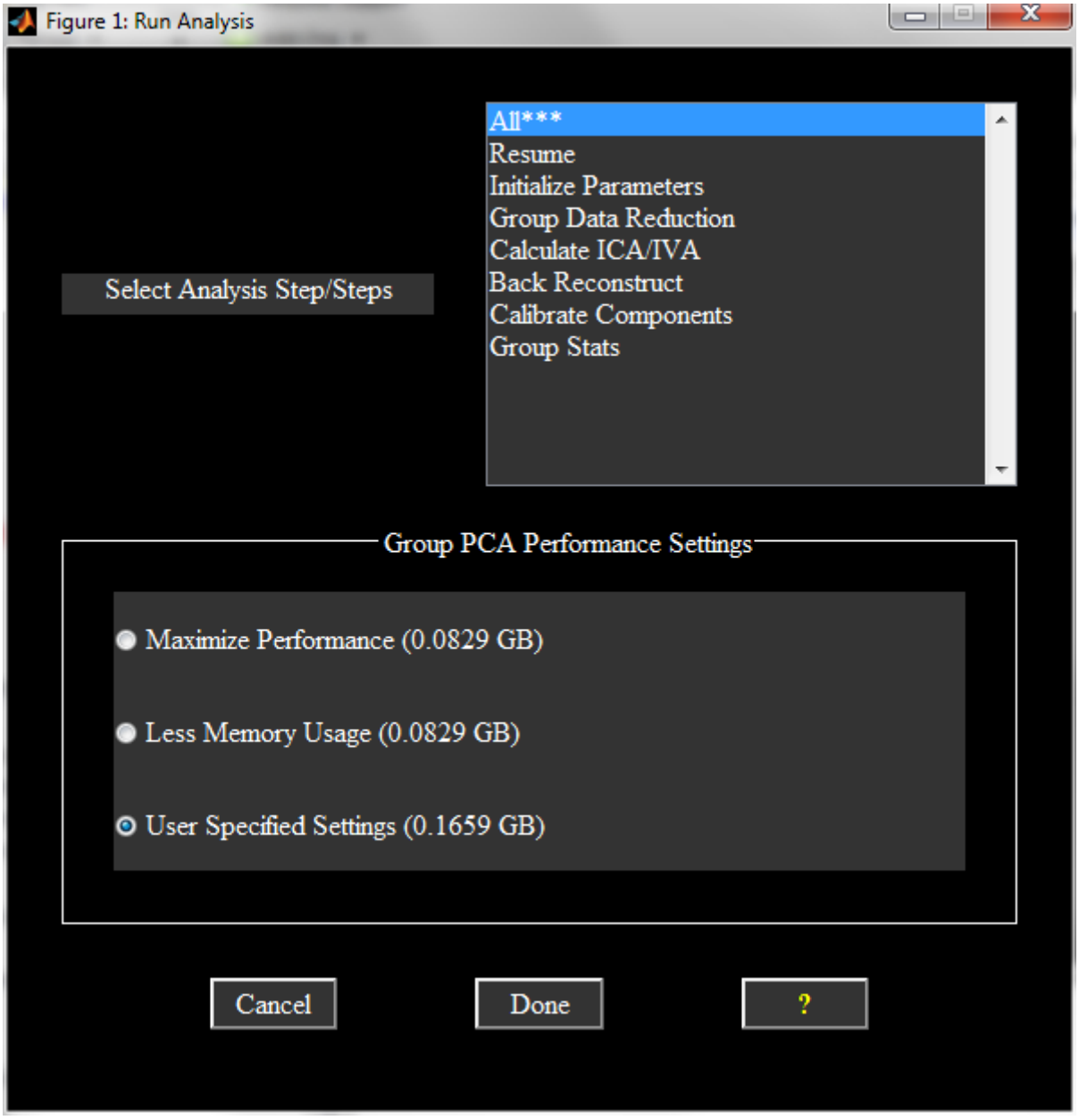

Figure 4-3 Analysis Steps

4.1.1 FastICA

On all experiments using FastICA, the default parameters were used, 16 components were extracted and projected on a high-resolution Colin template brain, the $tanh$ nonquadratic nonlinearity function $G(u)$ was used (Eq 16) and the data were

preprocessed with PCA and whitened. Only FastICA will be shown in single run to demonstrate the existence of artifacts due to the components not being optimally separated.

4.1.1.1 Single run

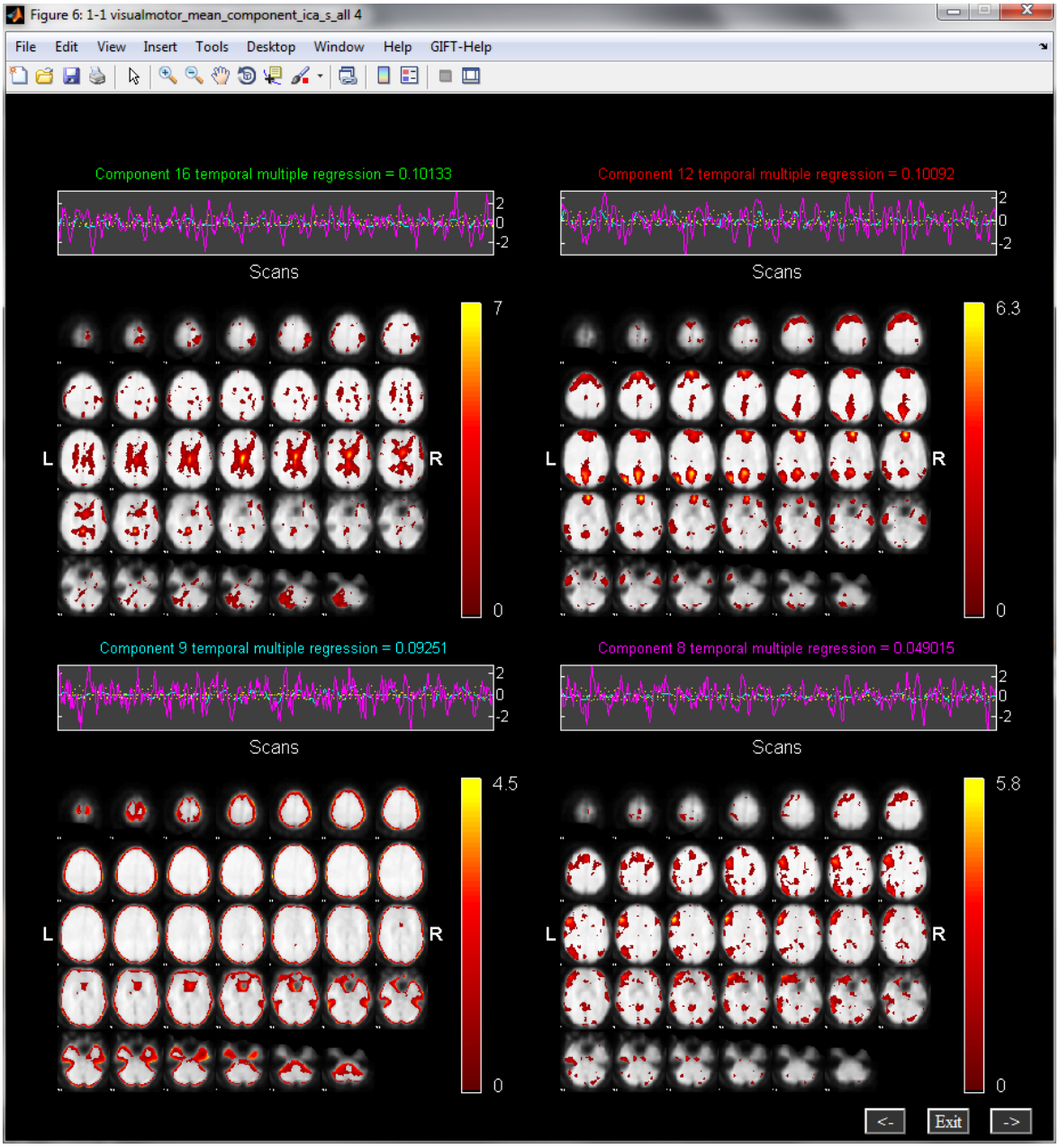

Figure 4-4 Selected projections of 4 components on a low-resolution template brain after being sorted on a temporal manner using multiple regression on all data on all timecourses. (Upper left) Component resembling the Medial Visual network, (upper right) definite component of DMN network, (Lower left) component depicting noise, (lower right) undefined component, resembles fronto-parietal networks

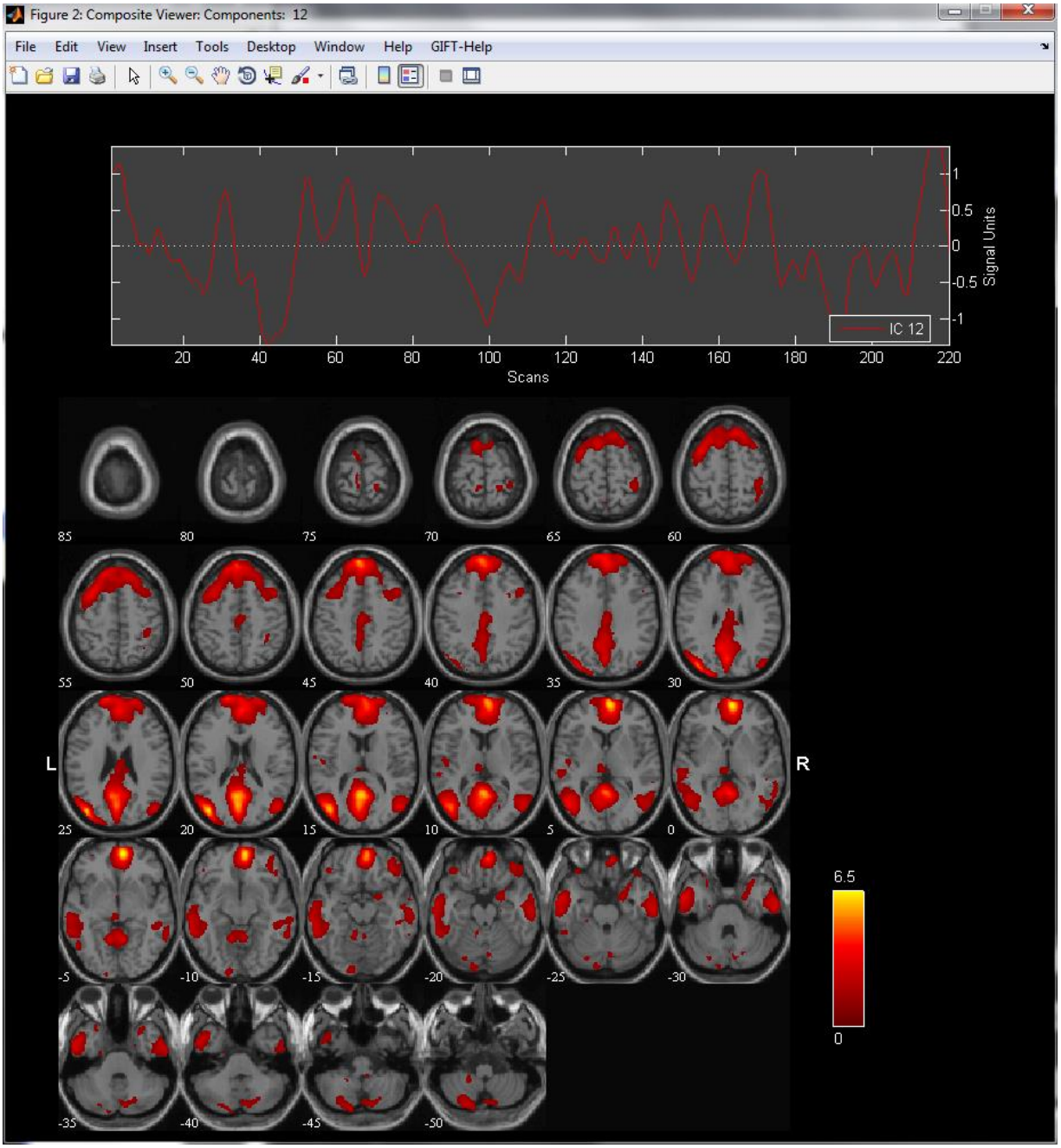

Figure 4-5 Anatomical projection of extracted mean IC of DMN functional network

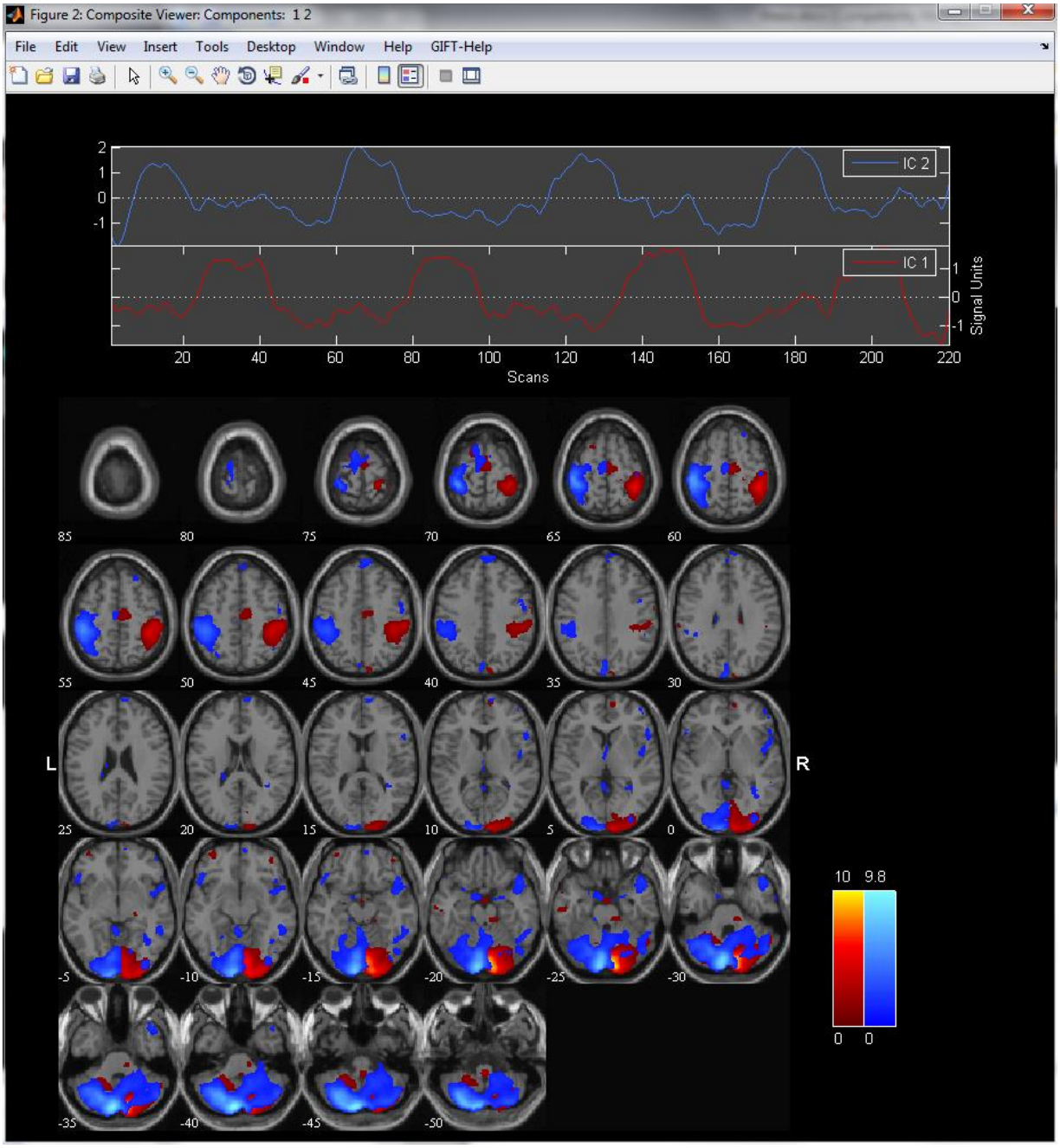

Figure 4-6 Composite projection of 2 IC representing left and right parts Visual and motor networks.

Due to the nature of the paradigm (Appendix), the alternating visual stimuli and the simultaneous motor task can be seen on Figure 4-6.

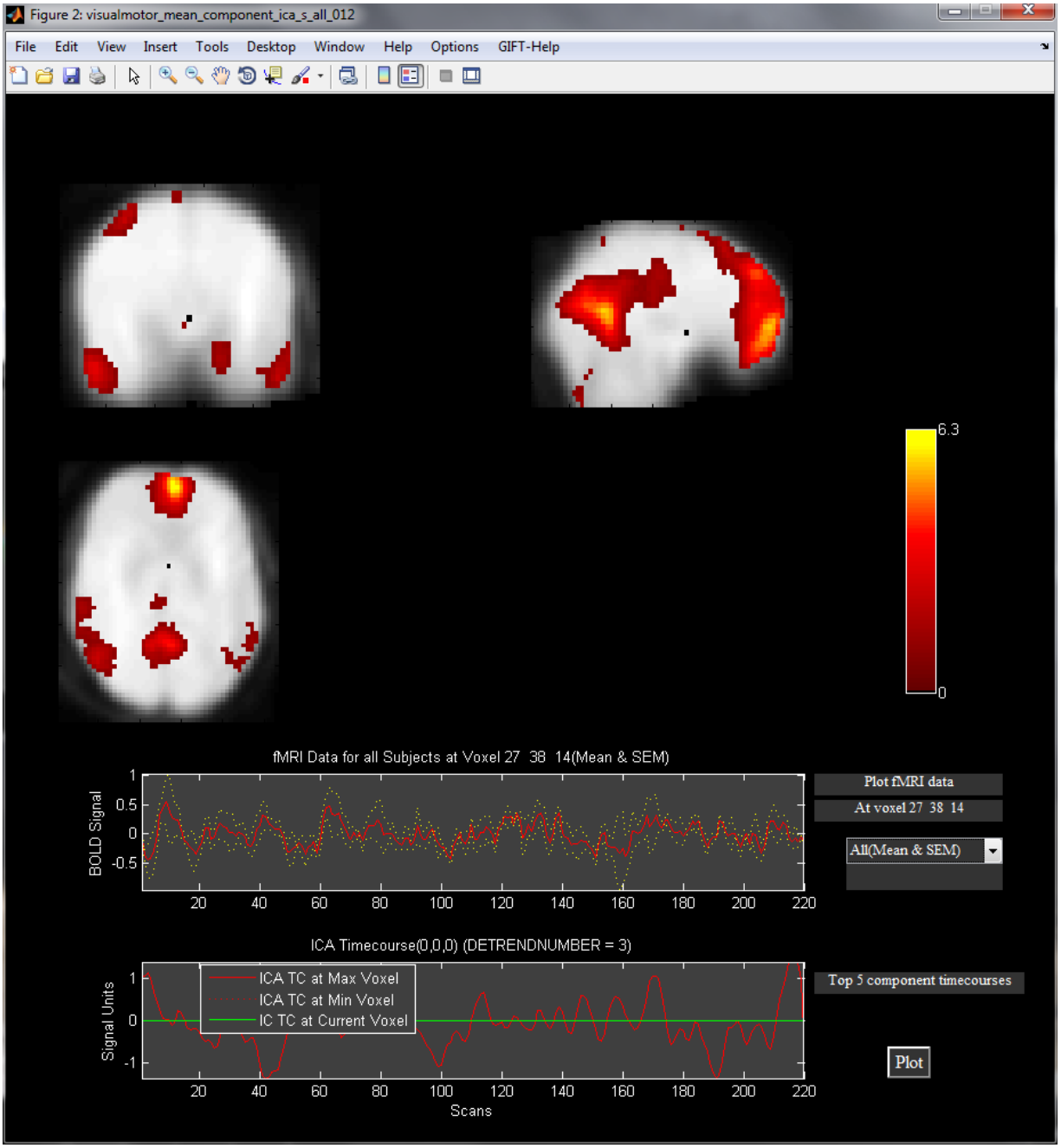

Figure 4-7 Projection of mean DMN component of all subjects and the corresponding time course

It has to be noted, that a single-run ICA doesn't always bring good results and multiple runs with the selection of the persistent components (refined from artifacts and random components) is recommended.

4.1.1.2 ICASSO

Same setting with the single run was used with Random initialisation and ICA was run 15 times. ICASSO compared for similarity and ranked the components as shown on the following Figures.

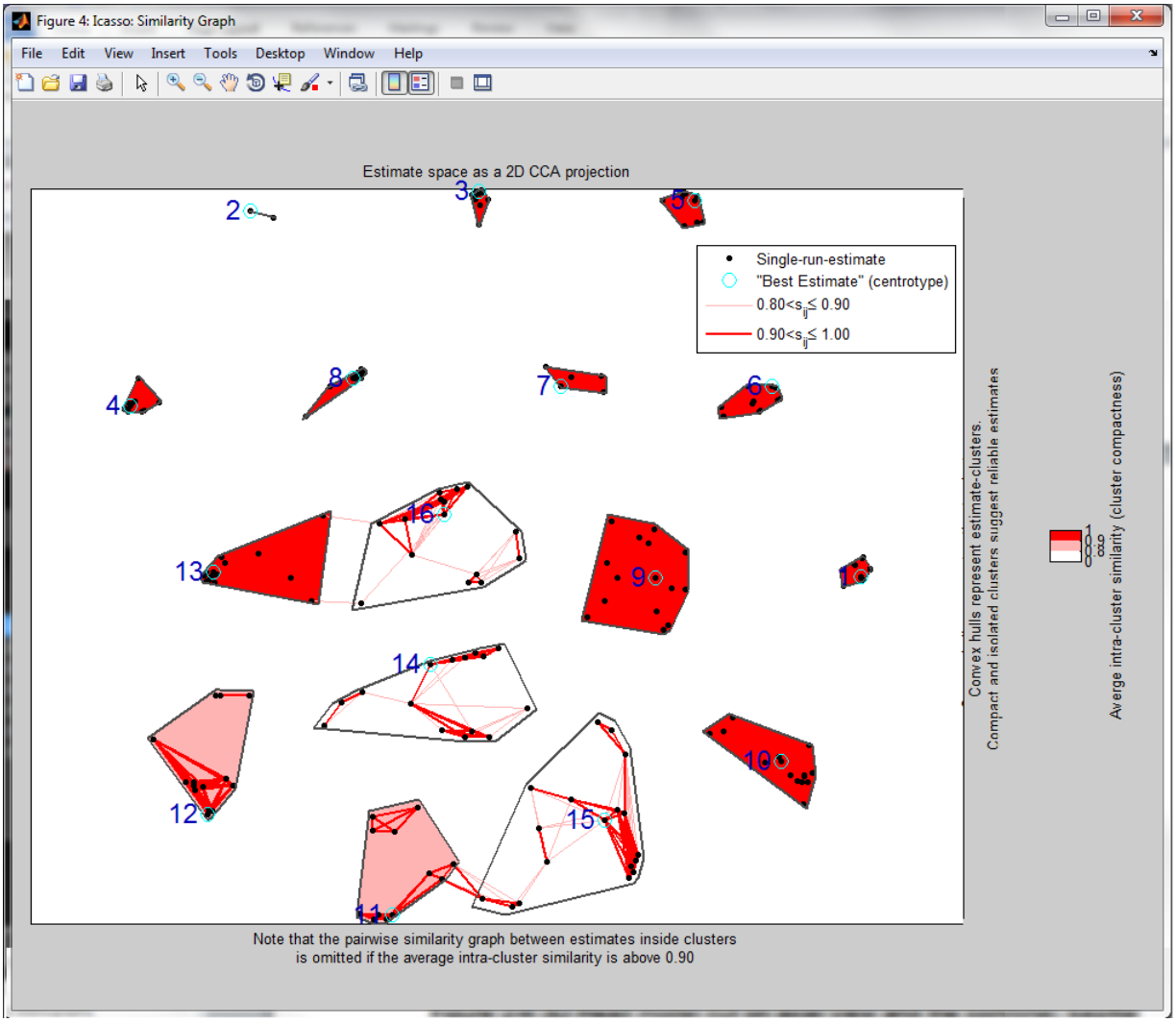

Figure 4-8 ICASSO Similarity Graph after 15 runs on 16 components

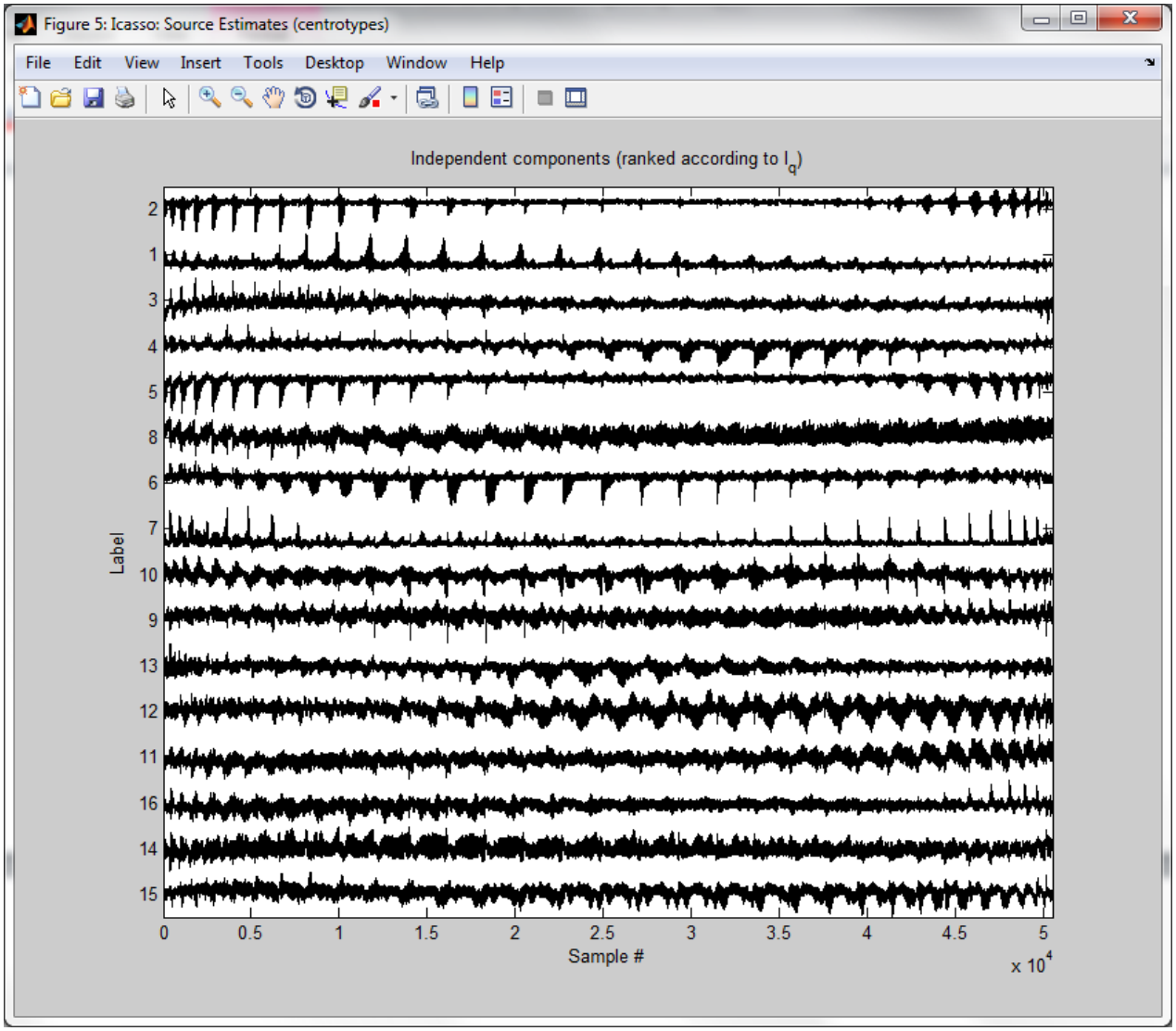

Figure 4-9 Ranking of components

Components 1-10 were very similar on all 15 runs and one can see on Figure 4-10 both left and right visuomotor networks and the anterior executive network. Another interesting phenomenon is when a component is split in two, as happens on Figure 4-11 on the DMN network. On the composite image (Figure 4-12) of the components one can see the spatial and temporal overlap creating the DMN network.

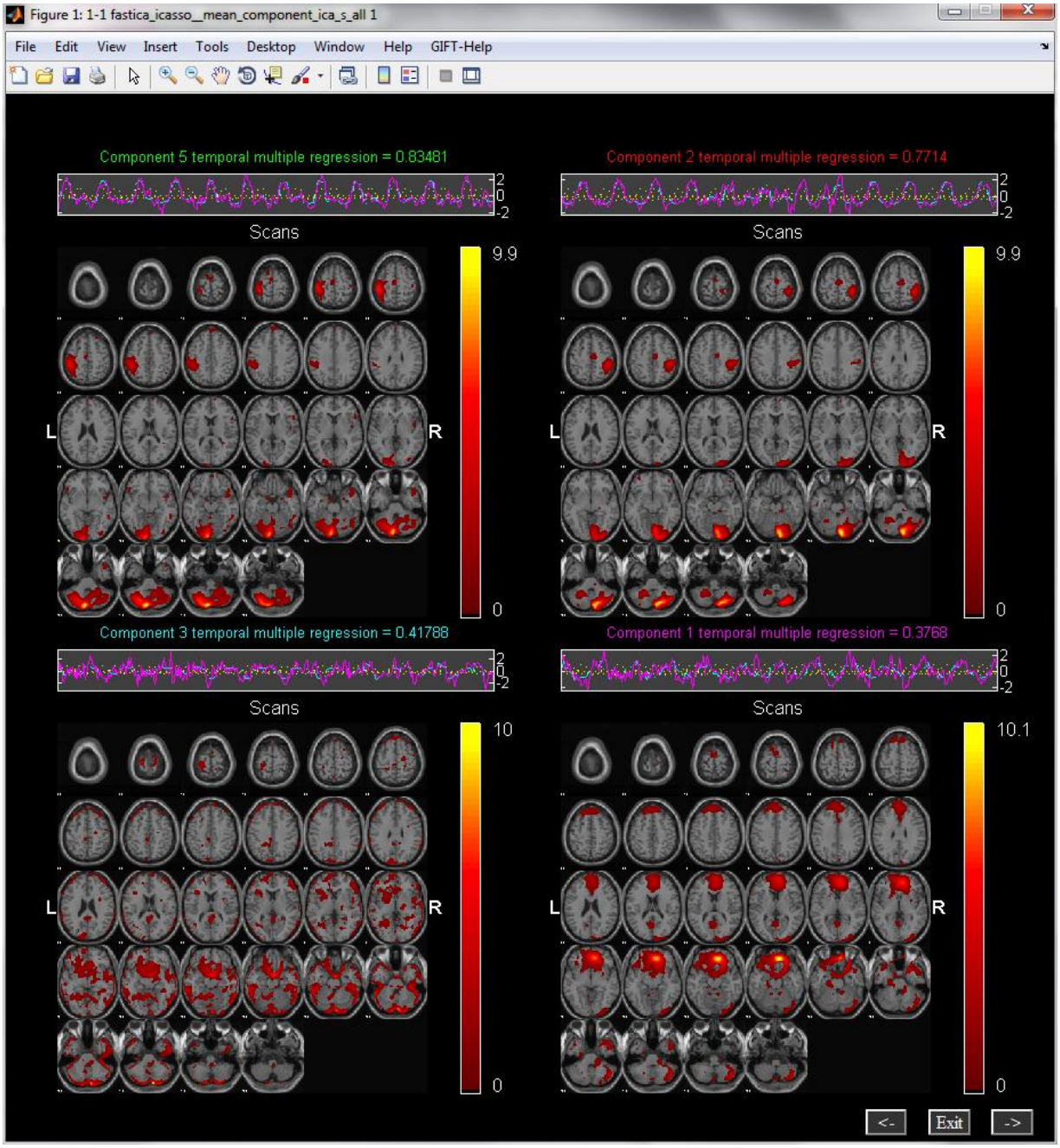

Figure 4-10 Selected projections of 4 components after being sorted on a temporal manner using multiple regression on all data on all timecourses. (Upper) Left and right visuomotor networks, (Lower right) Anterior executive network

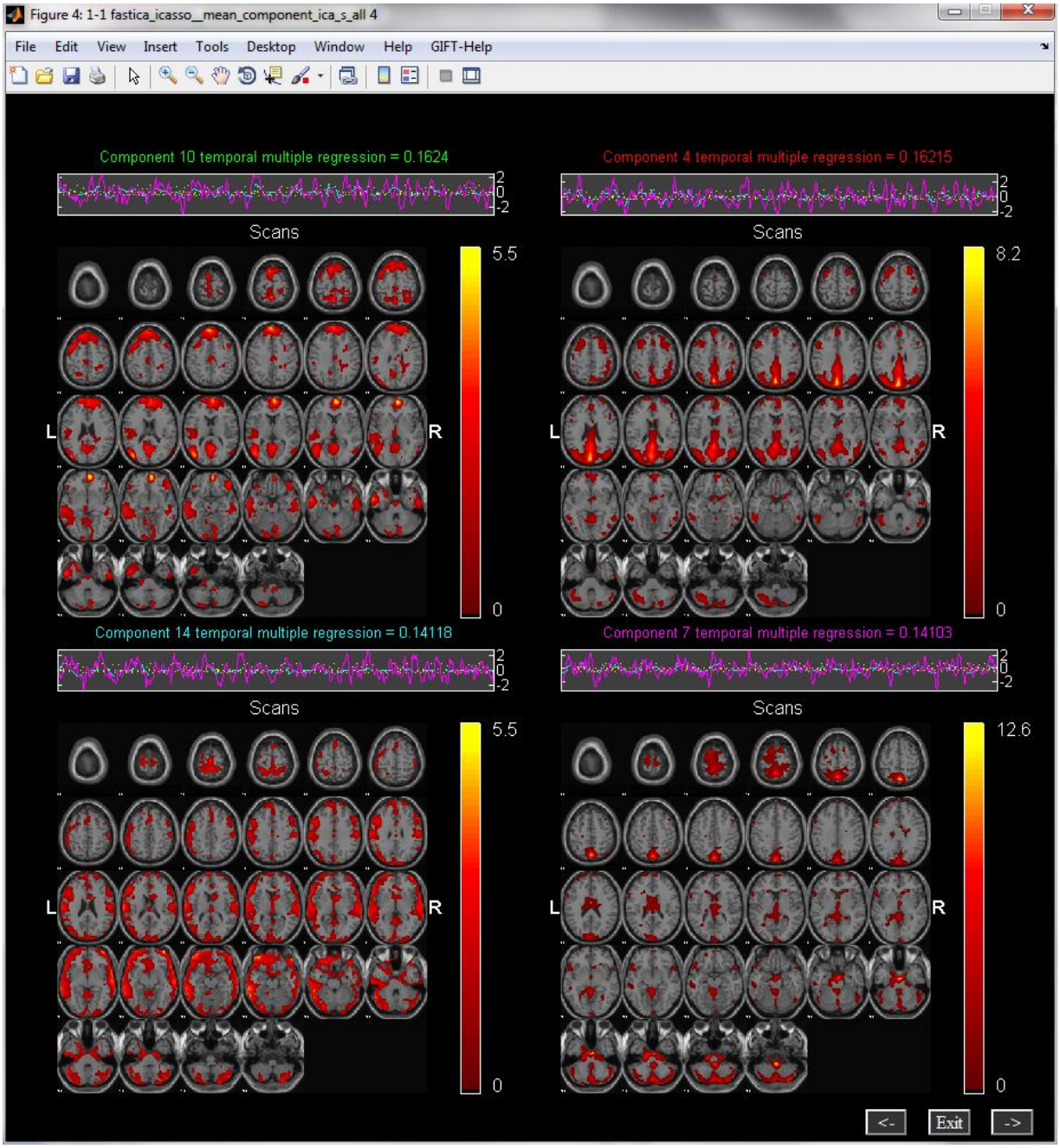

Figure 4-11 Selected projections of 4 components after being sorted on a temporal manner using multiple regression on all data on all timecourses. (Upper) the DMN network has been split into 2 components, (Lower right) component resembles attention network

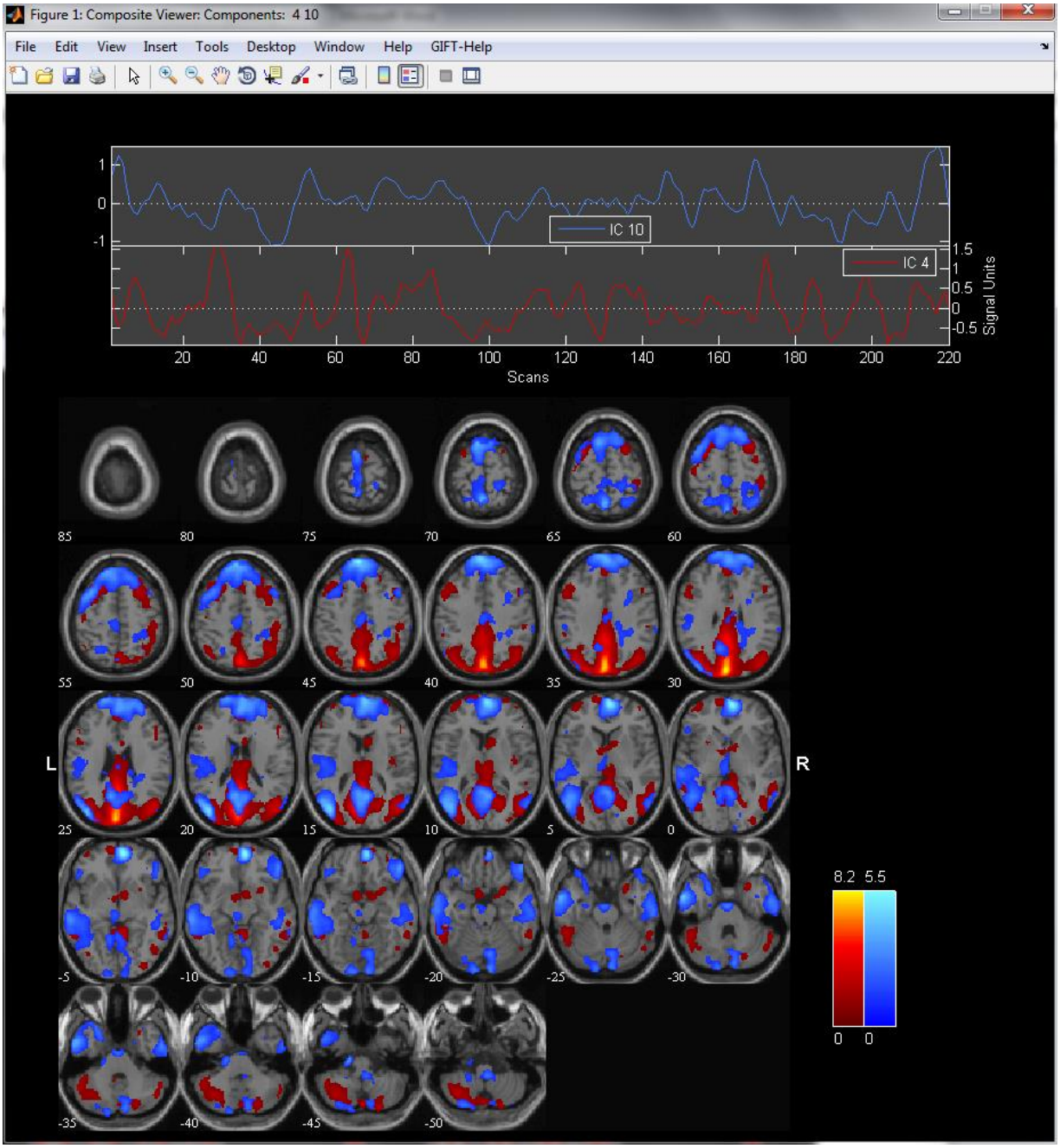

Figure 4-12 Composite image of components reconstructing split DMN using FastICA

4.1.2 INFOMAX

Same setting with the FastICA single run was used with Random initialisation and ICA was run 15 times. ICASSO compared for similarity and ranked the components as shown on the following Figures.

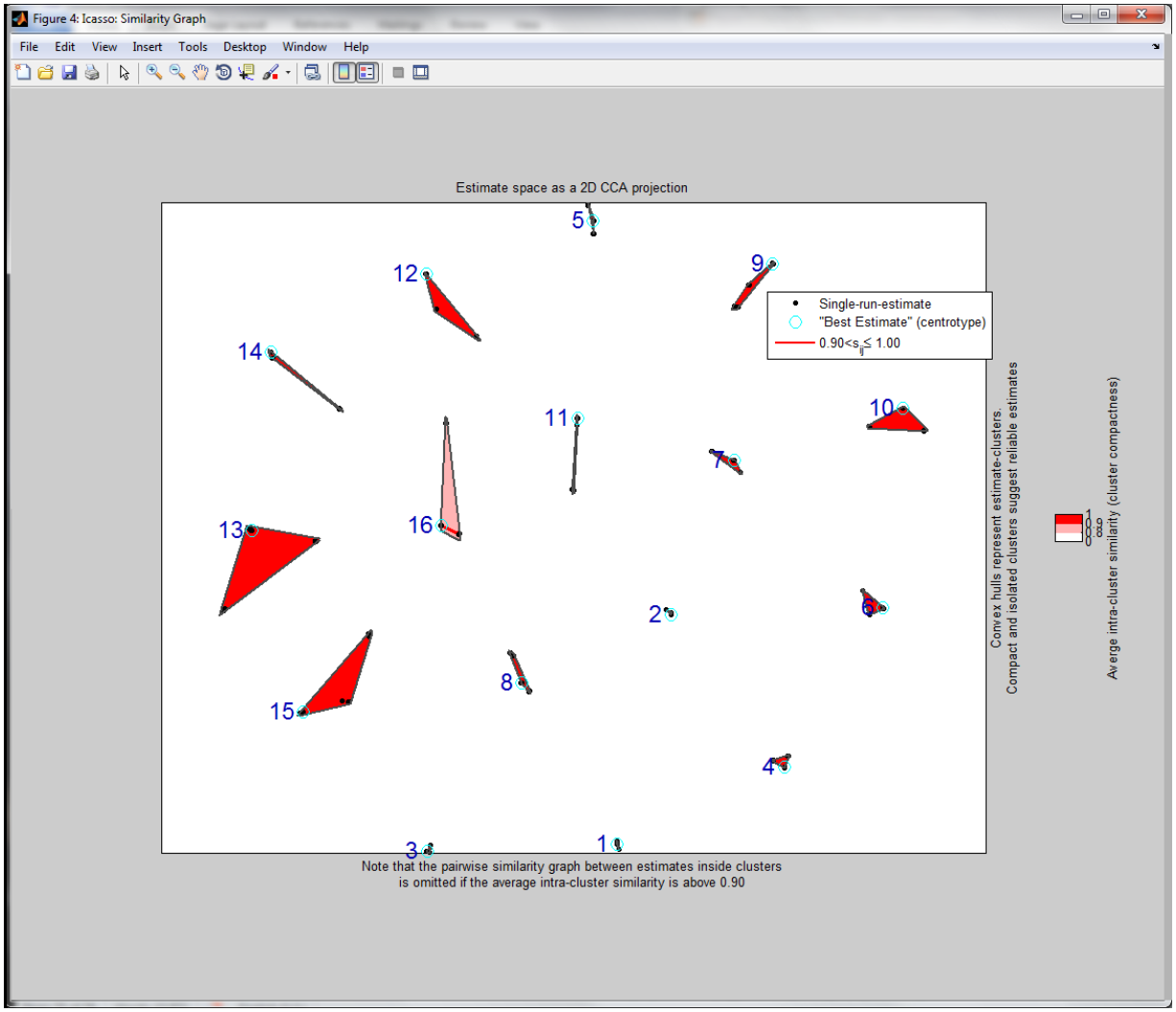

Figure 4-13 Similarity Graph after 15 runs on 16 components

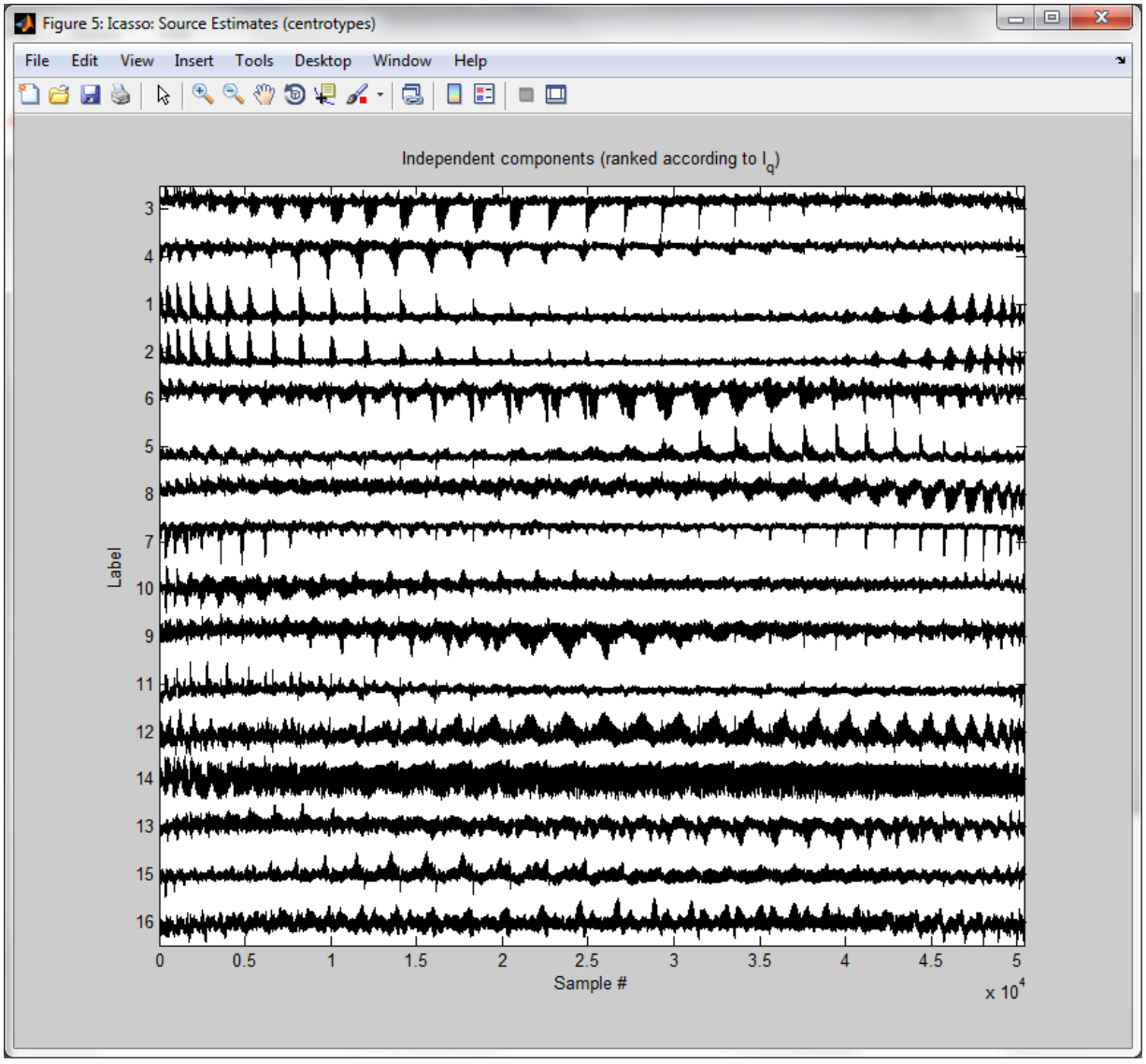

Figure 4-14 Ranking of components

Infomax after 15 runs and on 16 components yielded very good results as shown on the following Figures. The components were sorted and the top four were both left and right Visual networks, anterior executive network and the motor network. Also, two other Visual components were detected, the posterior executive network and the DMN.

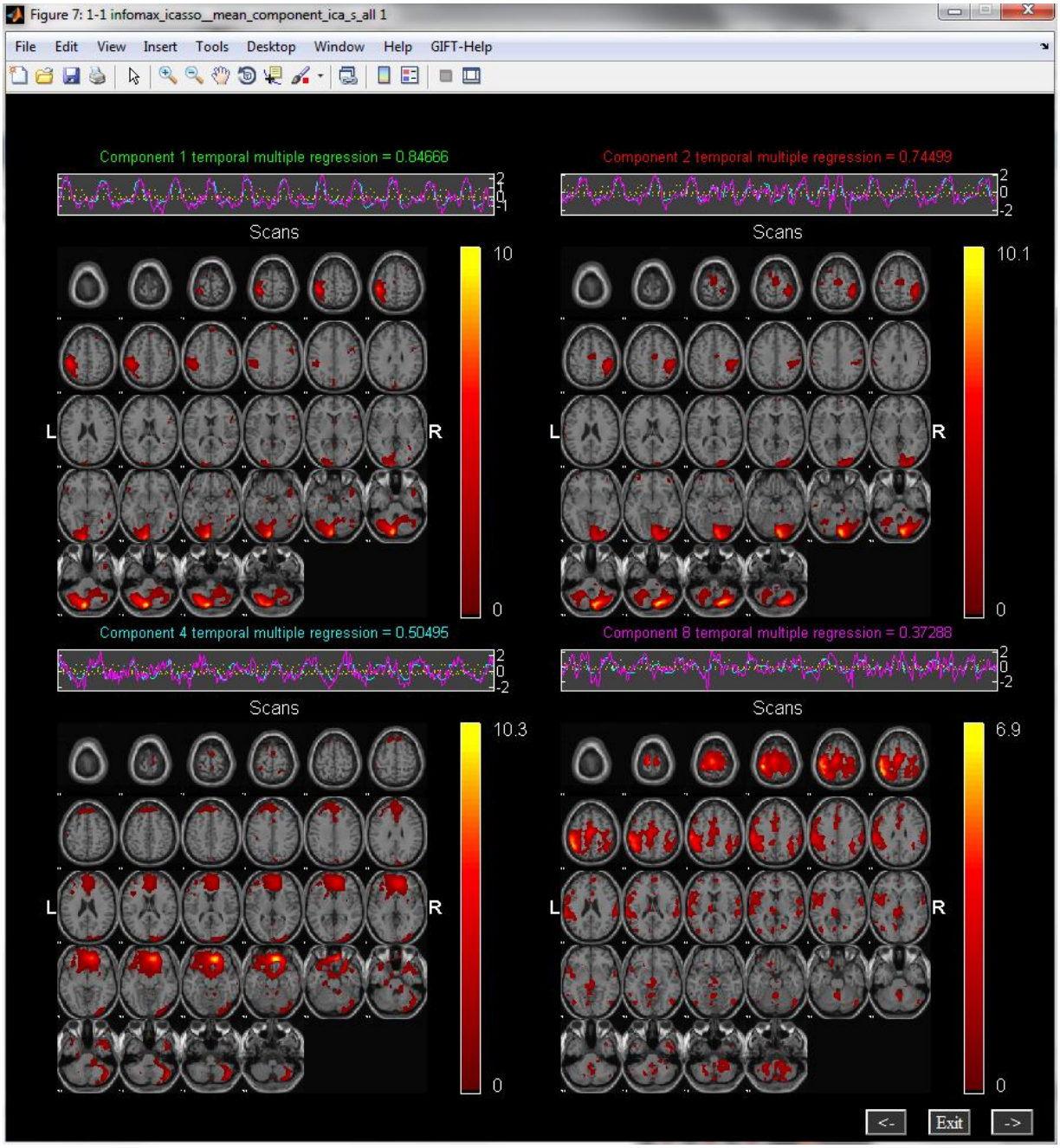

Figure 4-15 Selected projections of 4 components after being sorted on a temporal manner using multiple regression on all data on all timecourses. (Upper) Left and right visuomotor networks, (Lower left) Anterior executive network, (lower right) motor network.

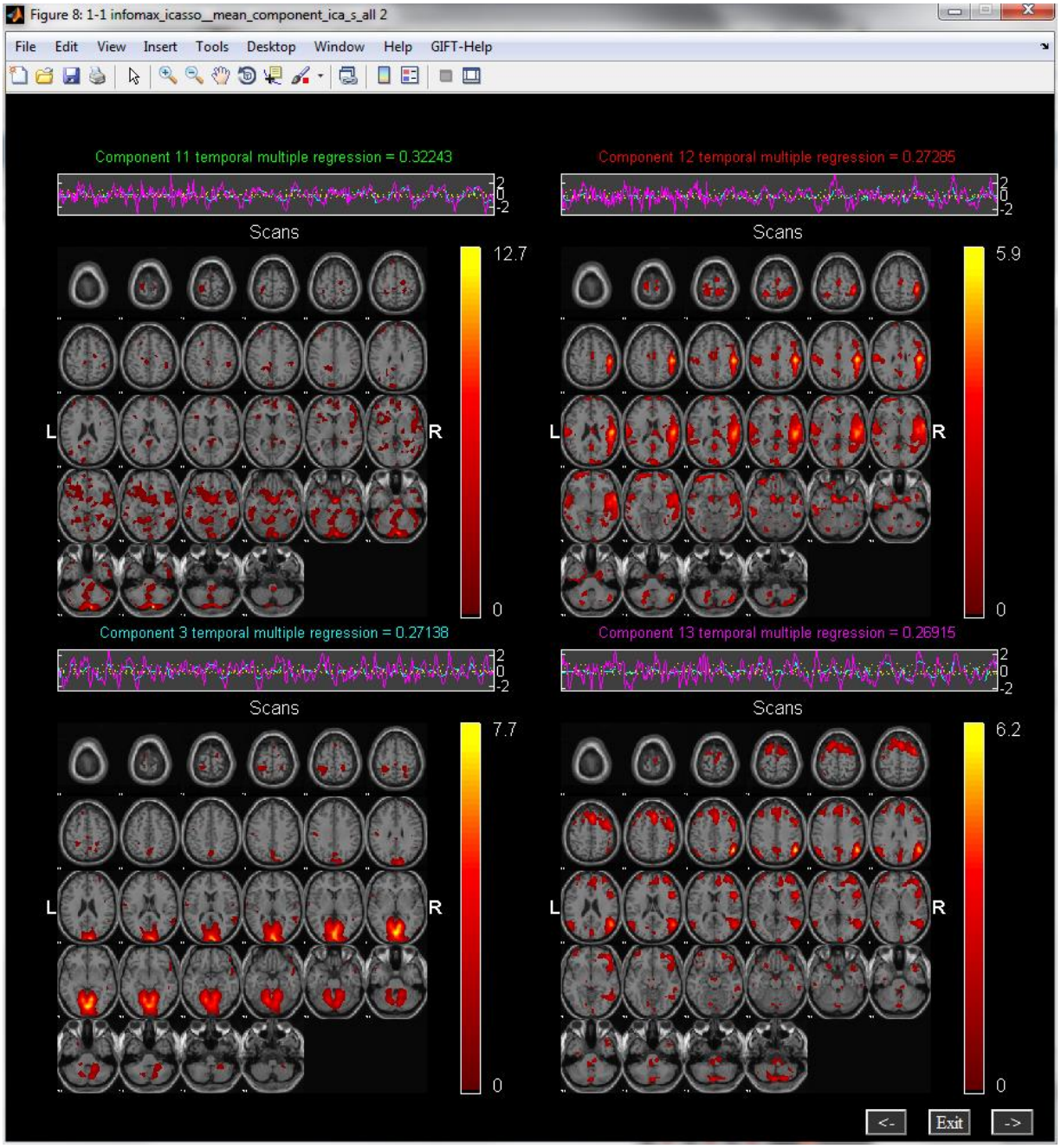

Figure 4-16 Selected projections of 4 components after being sorted on a temporal manner using multiple regression on all data on all timecourses. (Lower left) Central visual network, (Lower right) Posterior executive network

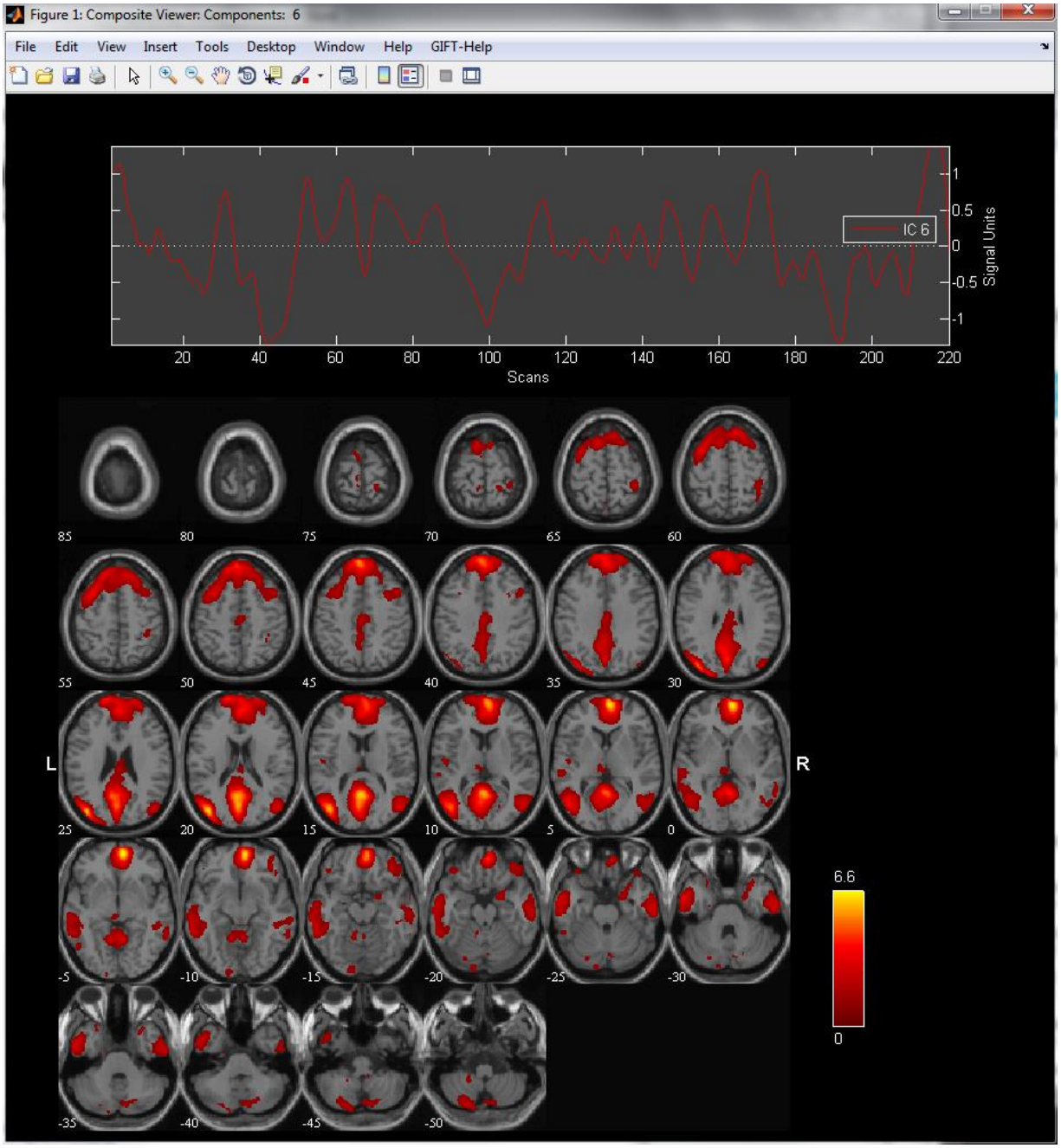

Figure 4-17 Anatomical projection of extracted mean IC of DMN functional network using Infomax

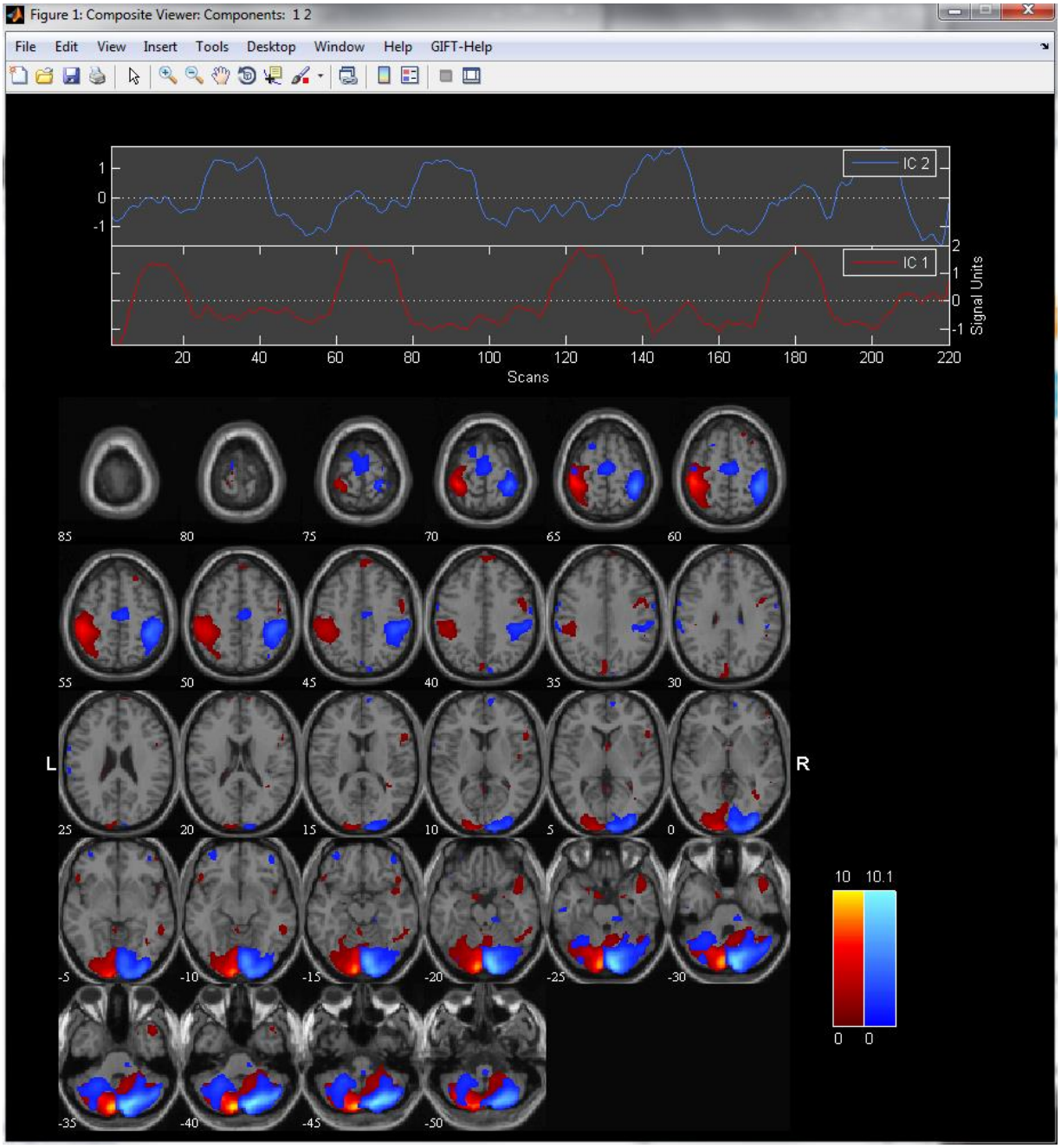

Figure 4-18 Composite image of visuomotor components demonstrating the alternating mirrored activation

5 Bibliography and Recommended reading

1. Abeles M, Local Cortical Circuits (1982) New York: Springer-Verlag.
2. Amari, S. I. (1999). Natural gradient learning for over-and under-complete bases in ICA. *Neural Computation*, *11*(8), 1875-1883.
3. Augustine, M. P., Wong-Foy, A., Yarger, J. L., Tomaselli, M., Pine, A., TonThat, D. M. and Clarke, J. "Low field magnetic resonance images of polarized noble gases obtained with a dc superconducting quantum interference device," Applied Physics Letters 72, 1908 (1998)
4. Baillet, S Garnero L (1997) A Bayesian Approach to Introducing Anatomo-Functional Priors in the EEG/MEG Inverse Problem. IEEE Trans. Biomed. Eng. 44:374-385.
5. Barnes GR, Furlong PL, Singh KD, Hillebrand A (2006) A verifiable solution to the MEG inverse problem. Neuroimage 31(2):623-626.
6. Bell, A. J., & Sejnowski, T. J. (1995). An information-maximization approach to blind separation and blind deconvolution. *Neural computation*, *7*(6), 1129-1159.
7. Belliveau J.W., Kennedy D.N., McKinstry R.C, Buchbinder B.R., Weisskoff R.M., Cohen M.S., Vevea J.M., Brady T.J. and Rosen B.R., (1991) Functional mapping of the human visual cortex by magnetic resonance imaging. Science. 254 (5032) 716-9.
8. Belouchrani, A., Abed-Meraim, K., Cardoso, J. F., & Moulines, E. (1997). A blind source separation technique using second-order statistics. *Signal Processing, IEEE Transactions on*, *45*(2), 434-444.
9. Braitenberg V and Schuz A (1991) Anatomy of the Cortex. Statistics and Geometry. New York: Springer-Verlag.
10. Braunwald E., *Heart Disease: A Textbook of Cardiovascular Medicine*, Fifth Edition, Philadelphia, W.B. Saunders Co., 1997
11. Calhoun, V. D., Adali, T., Pearlson, G. D., & Pekar, J. J. (2001). A method for making group inferences from functional MRI data using independent component analysis. *Human brain mapping*, *14*(3), 140-151.

12. Calhoun, V. D., Adali, T., Pekar, J. J., & Pearlson, G. D. (2003). Latency (in) sensitive ICA-Group independent component analysis of fMRI data in the temporal frequency domain. *NeuroImage*, *20*(3), 1661-1669.
13. Calhoun, V. D., Adalı, T., & Pekar, J. J. (2004). A method for comparing group fMRI data using independent component analysis: application to visual, motor and visuomotor tasks. *Magnetic resonance imaging*, *22*(9), 1181-1191.
14. Cardoso, J. F., & Souloumiac, A. (1993, December). Blind beamforming for non-Gaussian signals. In *Radar and Signal Processing, IEE Proceedings F*(Vol. 140, No. 6, pp. 362-370). IET.
15. Cohen D (1968) Magnetoencephalography: evidence of magnetic fields produced by alpha-rhythm currents. Science 161:784–786.
16. Cohen D, Schläpfer U, Ahlfors S, Hämäläinen S, Halgren E (2002) New Six-Layer Magnetically-Shielded Room for MEG. Proceedings of Biomag 2002.
17. Cruces, S., Castedo, L., & Cichocki, A. (2000). Novel blind source separation algorithms using cumulants. In *Acoustics, Speech, and Signal Processing, 2000. ICASSP'00. Proceedings. 2000 IEEE International Conference on* (Vol. 5, pp. 3152-3155). IEEE.
18. Cruces, S., Cichocki, A., & Amari, S. I. (2001). Criteria for the simultaneous blind extraction of arbitrary groups of sources. In *Proc. Int. Conf. on ICA and BSS* (pp. 740-745).
19. Démonet J.F., Thierry G. and Cardebat D., (2005) Renewal of the Neurophysiology of Language:Functional Neuroimaging Physiol Rev 85:49-95
20. Diamantaras, K. I., & Kung, S. Y. (1996). *Principal component neural networks*. New York: Wiley.
21. Edelman GM and Tononi G (2000) A Universe of Consciousness, New York: Basic Books.
22. Fox M.D. and Raichle M.E., (2007) Spontaneous fluctuations in brain activity observed with functional magnetic resonance imaging. Nature Review Neuroscience 8 700-711
23. Freeman WJ (1975) Mass Action in the Nervous System, New York: Academic Press

24. Friston K.J., Holmes A., Worsley K.J., Poline J-B., Frith C.D. and Frackowiak R.S.J. (1995) Statistical parametric maps in functional imaging: a general linear approach. . Hum Brain Map 2: 189–210
25. Garroway AN. Grannell PK, Mansfield P. (1974) Image formation in NMR by a selective irradiative process. J Phys C: Solid State Phys
26. Georgiev, P., & Cichocki, A. (2001). Blind source separation via symmetric eigenvalue decomposition. In *Signal Processing and its Applications, Sixth International, Symposium on. 2001* (Vol. 1, pp. 17-20). IEEE.
27. H. Hotelling. *Analysis of a Complex of Statistical Variables into Principal Components*. J. Educ. Psych., 24:498–520, 1933.
28. Huettel, S. A.; Song, A. W.; McCarthy, G. (2009), Functional Magnetic Resonance Imaging (2 ed.), Massachusetts: Sinauer, ISBN 978-0-87893-286-3
29. Hurst J.W.; *Naming of the waves in the ECG, with a brief account of their genesis*, Circulation 98 1998 1937-1942
30. Hyvärinen, A., & Oja, E. (1997). A fast fixed-point algorithm for independent component analysis. *Neural computation*, *9*(7), 1483-1492.
31. Hyvarinen, A. (1999). Fast and robust fixed-point algorithms for independent component analysis. *Neural Networks, IEEE Transactions on*, *10*(3), 626-634.
32. Hyvärinen, A.; Oja, E. (2000): *Independent Component Analysis: Algorithms and Application* , Neural Networks, 13(4-5):411-430.
33. Hyvärinen, A.; Karhunen, J.; Oja, E. (2001): *Independent Component Analysis,* New York: Wiley, ISBN 978-0-471-40540-5, Chapter 6
34. Jirsa VK and Haken H (1997) A derivation of a macroscopic field theory of the brain from the quasi-microscopic neural dynamics. Physica D 99: 503-526.
35. Jolliffe, I. T. (2002). *Principal component analysis*. Springer verlag. p. 28
36. Katznelson RD (1981) Normal modes of the brain: Neuroanatomical basis and a physiological theoretical model. In PL Nunez (Au), Electric Fields of the Brain: The Neurophysics of EEG, 1st Edition, New York: Oxford University Press, pp 401-442.
37. Klein, S.; Thorne, B. M. (3 October 2006). *Biological psychology*. New York, N.Y.: Worth. ISBN 0-7167-9922-7.

38. Koldovsky, Z., Tichavsky, P., & Oja, E. (2006). Efficient variant of algorithm FastICA for independent component analysis attaining the Cramér-Rao lower bound. *Neural Networks, IEEE Transactions on*, *17*(5), 1265-1277.
39. Lauterbur, P.C.:Image Formation by Induced Local Interactions: Examples Employing Nuclear Magnetic Resonance, Nature 242190-191 (1973)
40. Le Bihan D., Urayama S., Aso T., Hanakawa T., and Fukuyama H., (2006) Direct and fast detection of neuronal activation in the human brain with diffusion MRI. PNAS 103 8263-8268
41. Lee, T. W., Girolami, M., & Sejnowski, T. J. (1999). Independent component analysis using an extended infomax algorithm for mixed subgaussian and supergaussian sources. *Neural computation*, *11*(2), 417-441.
42. Lin, Q. H., Zheng, Y. R., Yin, F. L., Liang, H., & Calhoun, V. D. (2007). A fast algorithm for one-unit ICA-R. *Information Sciences*, *177*(5), 1265-1275.
43. Lin, Q. H., Liu, J., Zheng, Y. R., Liang, H., & Calhoun, V. D. (2010). Semiblind spatial ICA of fMRI using spatial constraints. *Human brain mapping*, *31*(7), 1076-1088.
44. Logothetis N.K., Pauls J., Augath M., Trinath T. and Oeltermann A.(2001) Neurophysiological investigation of the basis of the fMRI signal. Nature 412 150-7
45. A. A. Miranda, Y. A. Le Borgne, and G. Bontempi. *New Routes from Minimal Approximation Error to Principal Components*, Volume 27, Number 3 / June, 2008, Neural Processing Letters, Springer
46. Niedermeyer E. and da Silva F.L. (2004). *Electroencephalography: Basic Principles, Clinical Applications, and Related Fields.* Lippincot Williams & Wilkins. ISBN 0-7817-5126-8.
47. Nunez PL, Srinivasan R (1981). *Electric fields of the brain: The neurophysics of EEG*. Oxford University Press.
48. Nunez PL (1995) Neocortical Dynamics and Human EEG Rhythms. New York: Oxford University Press.
49. Nunez PL and Silberstein RB (2001) On the relationship of synaptic activity to macroscopic measurements: Does co-registration of EEG with fMRI make sense? Brain Topography 13: 79-96.

50. Ogawa S., Menon R.S., Kim S.G. and Ugerbil K., (1998) On the characteristics of functional magnetic resonance imaging of the brain. Annual Review of Biophysics and Biomolecular Structure 27 447-474
51. Ogawa S., Lee T.M., Kay A.K. and Tank D.W., (1990) Brain Magnetic Resonance Imaging with Contrast Dependent on Blood Oxygenation Proc. Natl. Acad. Sci. (USA), 87, 9868-9872
52. Ogawa S., Tank D.W., R. Menon R.S., Ellermann J.M., Kim S. G., Merkle H. and Ugurbil K., (1992), Intrinsic Signal Changes Accompanying Sensory Stimulation: Functional Brain Mapping With Magnetic Resonance Imaging. Proc. Natl. Acad. Sci. (USA), 89, 5951-5955
53. Pantazis D, Nichols TE, Baillet S, Leahy RM (2005) A comparison of random field theory and permutation methods for the statistical analysis of MEG data. Neuroimage 25(2):383-94.
54. Pauling L. and Coryell C. D., (1936) The magnetic properties and structure of hemoglobin, oxyhemoglobin and carbonmonoxy hemoglobin. Proc. Nayl. Acad. Sci. (USA) 22, 210-216
55. Pearson, K. (1901). *On Lines and Planes of Closest Fit to Systems of Points in Space* (PDF). Philosophical Magazine 2 (11): 559–572.).
56. Raichle M. E., (2000) A brief history of human functional brain mapping. In Brain Mapping: The systems edited by Toga A.W. and Mazziotta J.C., Academic Press, pp33-75
57. Rangayyan, R. M. *Biomedical signal analysis*. United States of America: Wiley Inter-Science, 2002. Print.
58. Shumskaya, E., Andriessen, T. M., Norris, D. G., & Vos, P. E. (2012). Abnormal whole-brain functional networks in homogeneous acute mild traumatic brain injury. *Neurology*, *79*(2), 175-182.
59. Silberstein RB, Danieli F and Nunez PL (2003) Fronto-parietal evoked potential synchronization is increased during mental rotation, NeuroReport 14: 67-71.
60. Silberstein RB, Song J, Nunez PL and Park W (2004) Dynamic sculpting of brain functional connectivity is correlated with performance, Brain Topography 16: 240-254.

61. Srinivasan R and Petrovic S (2006) MEG phase follows conscious perception during binocular rivalry induced by visual stream segregation. Cerebral Cortex, 16: 597-608.

62. Srinivasan R, Nunez PL and Silberstein RB (1998) Spatial filtering and neocortical dynamics: estimates of EEG coherence. IEEE Transactions on Biomedical Engineering, 45: 814-825.

63. Sung Y.W., Kamba M. and Ogawa S., (2007) An fMRI study of the functional distinction of neuronal circuits at the sites on ventral visual stream co-activated by visual stimuli of different objects. Exp Brain Res. 181 657-63

64. Tatum, W. O., Husain, A. M., Benbadis, S. R. (2008) *Handbook of EEG Interpretation* Demos Medical Publishing.

65. Tong, L., Liu, R. W., Soon, V. C., & Huang, Y. F. (1991). Indeterminacy and identifiability of blind identification. *Circuits and Systems, IEEE Transactions on*, *38*(5), 499-509.

66. Towle VL, Bolaños J, Suarez D, Tan K, Grzeszczuk R, Levin DN, Cakmur R, Frank SA, Spire JP. (1993). *The spatial location of EEG electrodes: locating the best-fitting sphere relative to cortical anatomy*. Electroencephalogr Clin Neurophysiol 86 (1): 1–6. doi:10.1016/0013-4694(93)90061-Y. PMID 7678386.

67. Webb G.A., (2007) Editor, Modern Magnetic Resonance: Volumes 1-3 Springer Verlag

68. Whittingstall, K; Logothetis, NK. (2009). "Frequency-band coupling in surface EEG reflects spiking activity in monkey visual cortex". Neuron 64 (2): 281–9.

69. Yeredor, A. (2000). Blind separation of Gaussian sources via second-order statistics with asymptotically optimal weighting. *Signal Processing Letters, IEEE*,*7*(7), 197-200.

6 Appendix

6.1 fMRI data

The paradigm contains two identical but spatially offset, periodic, visual stimuli, shifted by 20 seconds from one another. The visual stimuli were projected via an LCD projector onto a rear-projection screen subtending approximately 25 degrees of visual field, visible via a mirror attached to the MRI head coil. The stimuli consisted of an 8 Hz reversing checkerboard pattern presented for 15 seconds in the right visual hemifield, followed by 5 seconds of an asterisk fixation, followed by 15 seconds of checkerboard presented to the left visual hemifield, followed by 20 seconds of an asterisk fixation. The 55 second set of events was repeated four times for a total of 220 seconds. The motor stimuli consisted of participants touching their right thumb to each of their four fingers sequentially, back and forth, at a self-paced rate using the hand on the same side on which the visual stimulus is presented. FMRI data from this paradigm, when analyzed with standard ICA, separates into two different task-related components (one in left visual and motor cortex, one in right visual and motor cortex).